AD NUMBER

AD857606

LIMITATION CHANGES

TO:

Approved for public release; distribution is unlimited.

FROM:

Distribution authorized to U.S. Gov't. agencies and their contractors; Critical Technology; JUL 1969. Other requests shall be referred to Rome Air Development Center, Attn: EMII0, Griffiss AFB, NY 13440. This document contains export-controlled technical data.

AUTHORITY

RADC ltr, 17 Sep 1971

RADC-TR-69-119
Final Technical Report
July 1969

ELECTRO OPTICS FOR ASSOCIATIVE STORAGE PROCESSOR

The Marquardt Corporation

Rome Air Development Center
Air Force Systems Command
Griffiss Air Force Base, New York

ELECTRO OPTICS FOR ASSOCIATIVE STORAGE PROCESSOR

Jacques M. Haniet
The Marquardt Corporation

FOREWORD

This final technical report was prepared by Jacques M. Hanlet of The Marquardt Corporation, Van Nuys, California, under USAF Contract No. F30602-68-C-0199, Project 5581, Task 558109. Secondary report number is TMC Report No. 25,286. The Rome Air Development Center project engineer was Mr. James Previte (EMIIO).

Distribution of this report is limited because the report represents advances in the state of the art which could prove useful to the Sino Soviet bloc.

This report has been reviewed and is approved.

Approved: James G. McGinnis
JAMES G. MCGINNIS, Major, USAF
Chief, Information Processing Branch

Approved: A E Stoll
A. E. STOLL, Colonel, USAF
Chief, Intel and Info Processing Division

FOR THE COMMANDER: Irving J. Gabelman
IRVING J. GABELMAN
Chief, Advanced Studies Group

ABSTRACT

A research and development program to develop materials and investigate their use in an electro optical associative processor. An analysis is performed to determine the compatibility between ferroelectric-photoconductor and light source from an energy viewpoint.

The material effort directed toward the development of thin film carrier injection electroluminescent materials is presented. The effort culminated with definition of a fabrication process for a P I N electroluminescent cell that can switch a ferroelectric element carrying a charge of approximately 10^{-9} microcoulombs in 30 microseconds.

TABLE OF CONTENTS

LIST OF ILLUSTRATIONS

SECTION I

INTRODUCTION

The objective of the contractual effort, described in this report, was to provide an electroluminescent material compatible with the associative storing processor, previously developed.

Several stringent considerations directed the choice of approach to be taken:

a. The short addressing time obtained in the ASP model prohibits the exploitation of field effect electroluminescence to achieve switching compatibility.

b. In order to match the photoconductor's spectral response, the carrier injection electroluminescence basis of this work had to rely on a II-VI compound host crystal.

c. As formerly described in report - USAF No. AF 30(602)3709, Project #8, Task #5581 - the model of ASP developed relied on batch production methods for the photoconductor and the ferroelectric films. Therefore, in order to be fully compatible, the electroluminescent devices should proceed from the same technology.

d. Since II-VI monocrystalline compounds are available only in small sizes, the main task was to produce electroluminescent junctions from epitaxial films over large areas.

The principal obstacles when dealing with II-VI compounds, pertain to polymorphism and unusually high point defects concentration from nonstoichiometric compositions - likewise, the production of efficient junctions from materials subject to self compensation present great difficulties from the device viewpoint.

Both polymorphism of structure and point defects density derive from processing technology. Both are susceptible to some control whereas self compensation cannot be disciplined in II-VI compounds. Self compensation prevents amphoteric conductivity in all but one of the II-VI compounds, viz. CdTe. Cadmium Telluride, however, has too narrow a band gap to give concordance between its radiative recombinations and the photoconductor response.

As a result of self compensation, low and unequal p,n, carrier concentrations preclude the formation of efficient homojunctions.

Only more or less broad heterojunctions are feasible in II-VI compounds; in conjunction with another program, two approaches to such structure were investigated in film form during this work.

SECTION II

ASP ELEMENTS COMPATIBILITY

1. BIT STRUCTURE

Two principal configurations for the ASP bit have been investigated and their performances reported in a previous report, USAF No. AF 30(602)3709, Project #8, Task 5581.

In correlating the present work, which concerns the optical means of address, reference will be made to the simplest structure for the bit shown in Figure 1 and for the word in Figure 2.

This bit configuration comprises three distinct electrical and optical paths accessible by spatial addressing. Only one path is used at any time either to store or detect for a binary "one" or a binary "zero". The third path is used to bypass the bit when it does not need to be addressed.

The spatial addressing is made with a light source located in the photoconductor vicinity, Figure 3, changing its conductivity from a very low to a high magnitude.

When the photoconductor is not illuminated, its very high resistance to current flow isolates the ferroelectric element from the voltage pulse, which remains undisturbed.

Under illumination the internal resistance of the photoconductor decreases to a point where the voltage pulse may be applied in its entirety to the ferroelectric element. Depending on the voltage pulse sign the ferroelectric element will then respond or not to the pulse interrogation. A complete model is shown in Figure 4.

The present task concerns the investigations of this light source.

2. ELEMENTS COMPATIBILITY

Storing or retrieving an information in a bit, comprising ferroelectric and photoconductor elements in series, with a voltage source, requires the flow of a charge Q.

The operation of storing or retrieving simply depends on the sign adopted by convention for this charge flow.

The charge Q can be delivered, depending on the photoconductor's ability to control this charge flow by changing its conductivity under illumination. Within the limits defined by processing characteristics, the change in conductivity will in turn depend upon the illumination intensity and the wavelength of the emitted light.

Each of the three elements constituting a bit are quantum devices and their degree of compatibility is based upon their respective quantum yields.

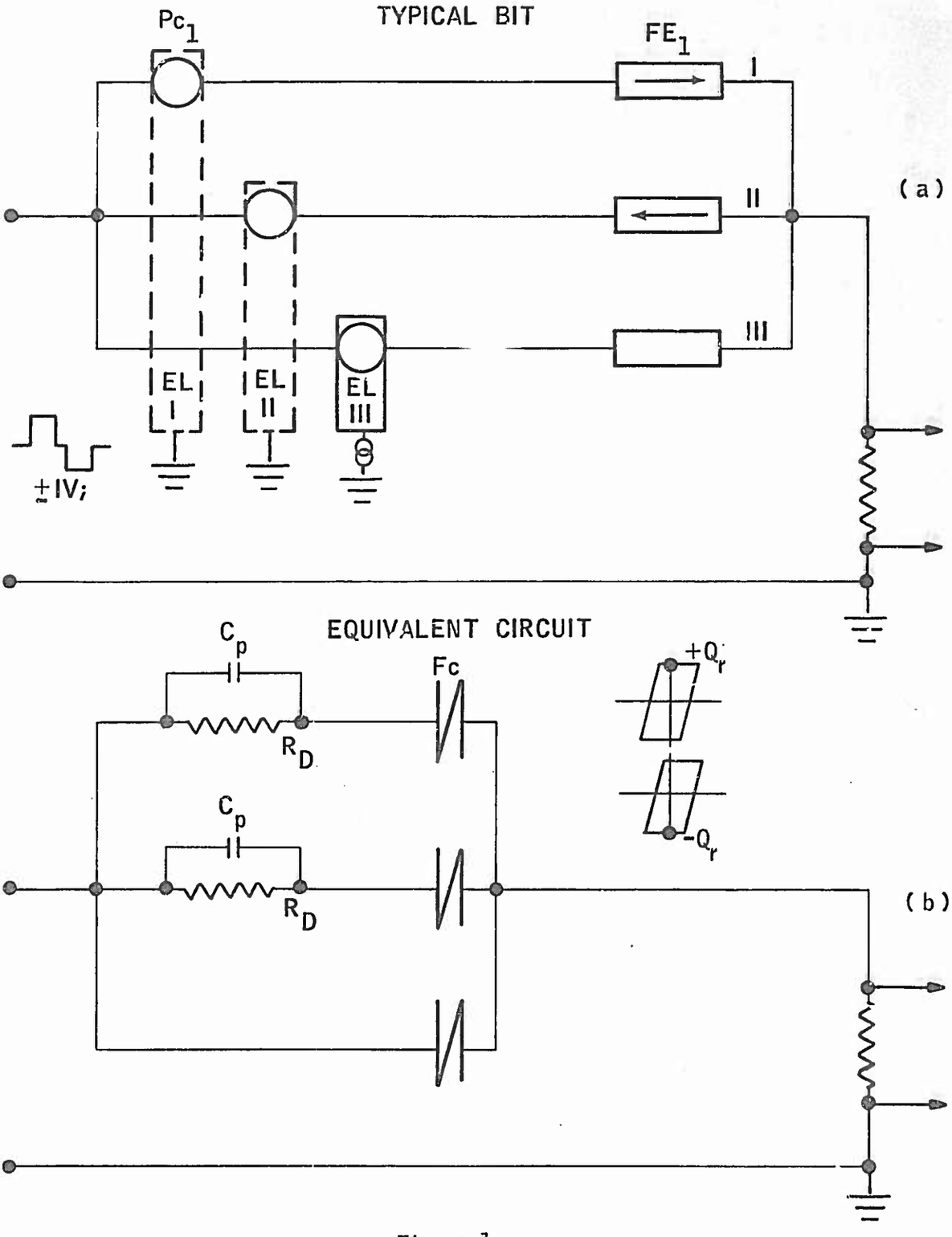

Figure 1

TYPICAL BIT STRUCTURE

R-21,229

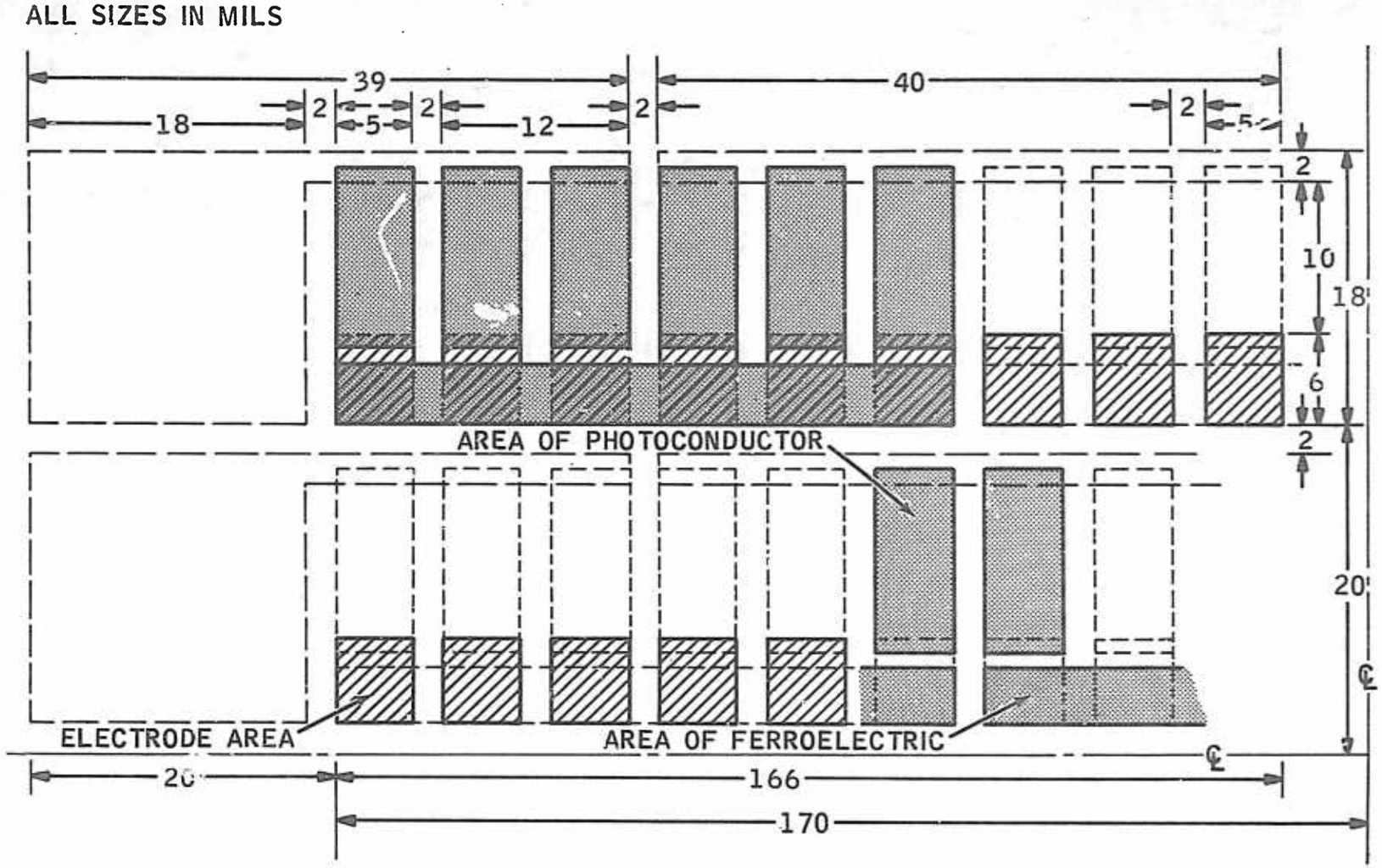

Figure 2

TYPICAL BIT WORD LAYOUT

R-23,828A

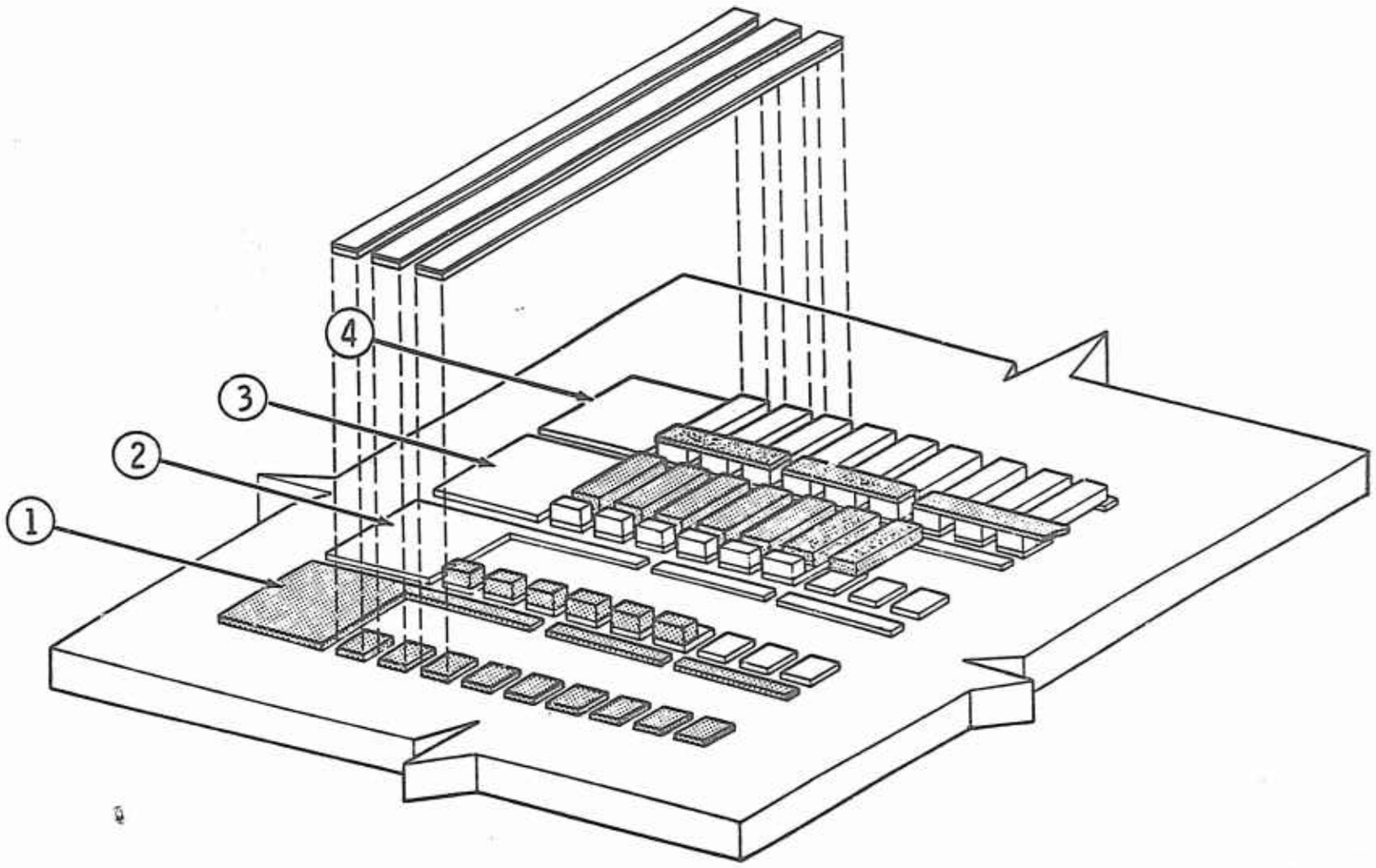

Figure 3

ASP CONFIGURATION

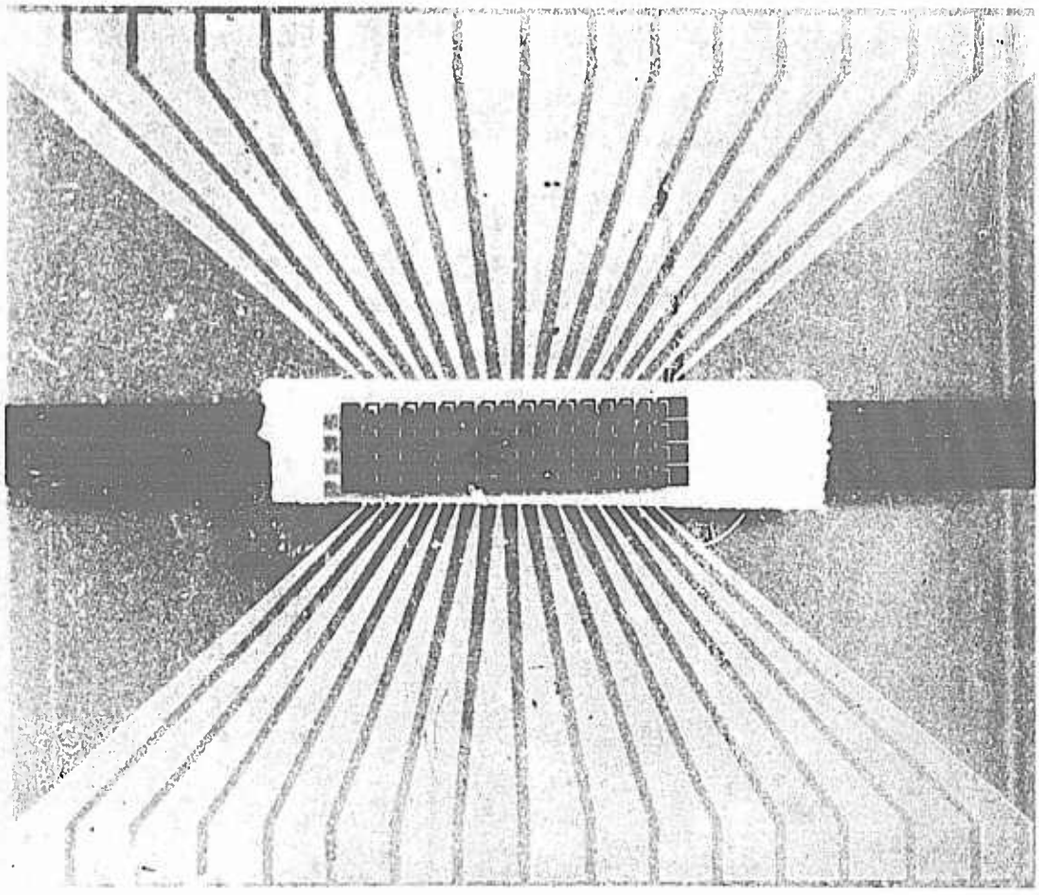

Figure 4

BIT WORD STRUCTURE

R-21,262
Neg. 6431-1

The charge Q of a particular ferroelectric depends on its maximum polarizability P_s in coulombs cm^{-2}, and the area A, in cm^2 devoted to the elementary bit,

$$Q = 2 P_s A_1 \quad \text{coulombs} \tag{1}$$

The energy level at which this charge is supplied to the bit is conditioned by the switching time requested from the ferroelectric element. At low electric field this switching time is given by the classical expression

$$t_s = t_o \exp \frac{\alpha d_1}{V_F} \quad \text{seconds} \tag{2}$$

with,

$$t_o = \frac{d_1^2}{\mu_1 V_F} \quad \text{seconds} \tag{3}$$

where: t_s = time taken for a complete polarization reversal under an applied voltage V_F.

d_1 = ferroelectric thickness in cm.

μ_1 = electric domain's mobility cm^2 $volt^{-1}$ sec^{-1}

α = activation potential volt cm^{-1}

The internal resistance of the voltage source V_F can be established on the basis of a constant current i, which in this case would give the charge Q as linear function of time. Hence, assuming a hysteresis loop of infinite squareness, the charge would be represented by,

$$Q = \int i dt \quad \text{coulombs} \tag{4}$$

In the pulse time interval t_s, the current flow does not remain constant but with most ferroelectrics the current goes through a maximum i_m at a time t_m as shown in Figure 5, and t_m assumes a value,

$$0.01\ t_s < t_m < t_s \tag{5}$$

Rather than solving eq (4) for i = Q/t between the limits $t = t_o$ to $t = t_s$, the network external resistance should be derived from the instantaneous current.

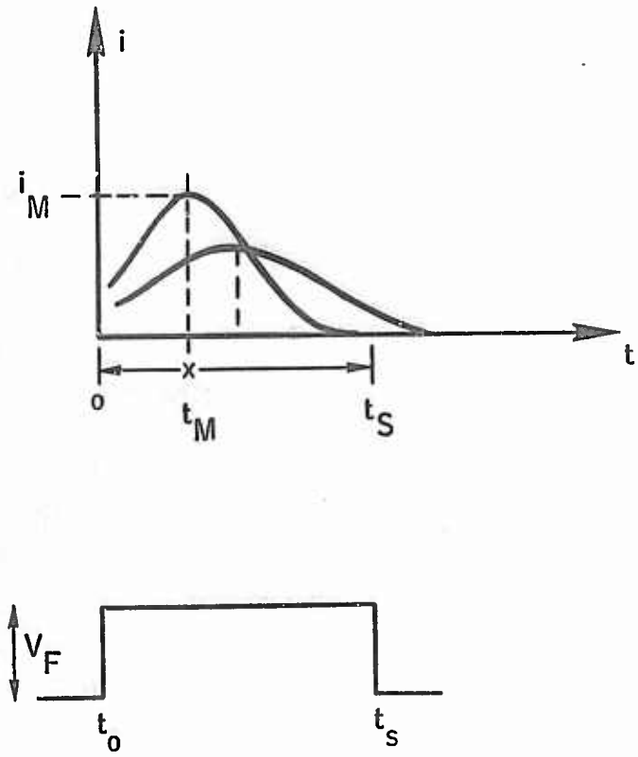

Figure 5

FERROELECTRIC SWITCHING TIME

$$i = Q \frac{t}{t_m^2} \exp \left[-\frac{1}{2} \left(\frac{t}{t_m} \right)^2 \right] \text{ amperes} \qquad (6)$$

$$\text{when } t = t_m \longrightarrow i_m = 0.6\, Q \frac{t}{t_m^2} \qquad (7)$$

Assuming the ferroelectric's losses negligible these equations characterize the operational parameters in storing or retrieving a bit.

The value obtained for i_m permits to define the power source requirements for a given switching time t_s.

According to Kirchhoff's law, since ferroelectric and photoconductor are series connected, the same current must flow through both devices.

Hence, compatibility between ferroelectric and photoconductor is assured, when,

$$i_m = \Delta \sigma V_p^{\beta} \qquad (8)$$

Where $\Delta\sigma$ represents the photoconductor increase in conductivity under the addressing light pulse.

The phenomenological exponent β affixed to the photoconductor voltage V_p assumes a value $1 < \beta < 2$ representing the contact electrodes properties with respect to the bulk photoconductor.

With an addressing light pulse of duration $t_L \leq t_s$ the change in conductivity $\Delta\sigma$ can be found from the relation

$$\Delta\sigma = \sigma_s \left(1 - \exp -\frac{t_L}{\tau_1}\right) \text{ mhos} \qquad (9)$$

Where σ_s represents the maximum conductivity attained at equilibrium, under constant illumination, i.e. when $t_L \gg \tau_i$ where τ_i is the instantaneous lifetime of the photons generated carriers.

For a constant photon density, the steady-state conductivity is given by,

$$\sigma_s = q\, \mu_2\, \tau K \phi \frac{L_2}{d_2 w_2} \eta \text{ mhos} \qquad (10)$$

with: q = electron charge 1.6×10^{-19} coulombs

μ_2 = photoconductor's electron mobility $cm^2\ volt^{-1}\ sec^{-1}$

τ = electron lifetime sec

ϕ = number of incident photons sec^{-1}, falling on the photoconductor's area, $A_2 = L_2 \times w_2$ cm^2

L_2 d_2 w_2 geometry, length, thickness, width, respectively

K = optical absorption coefficient

$$K = \frac{2.3}{d} \log \frac{1}{T_o}$$

T_o = photoconductor light transmission coefficient

η = quantum yield

The parameter τ can be calculated from experimental data in several ways, e.g. from the relation

$$\tau = \frac{1}{svp} \tag{12}$$

where: s = capture centers cross section for electrons,

$$s = 5 \times 10^{-25} N_o^{\,2} d_2^{\,-1} E_g^{\,2} \left(\frac{m}{m_e^* m_h^*}\right)^{\frac{3}{2}} \left(\frac{300}{T}\right)^{\frac{5}{2}} cm^2 \tag{13}$$

with: N_o = refractive index

E_g = band gap in electron volt

m = electron mass

m_e^* = effective electron mass

m_h^* = effective hole mass

T = absolute temperature

In eq (12) the thermal velocity v is obtained from,

$$v = \left(\frac{3kT}{m_o^*}\right)^{\frac{1}{2}} \quad \text{cm sec}^{-1} \tag{14}$$

with: k = Boltzmann's constant $1.38\ 10^{-16}$ erg $^{o}K^{-1}$ and p in (12) = density of capture centers.

The lifetime τ obtained from eq (12) will be the same as τ_i used in eq (9) only for a linear recombination, when the time constant of the exponential curve is equal to the lifetime τ.

Linear and quadratic photoconductors have been developed in the course of this program and a more general expression may be obtained for equilibrium and instantaneous lifetimes.

The experimental data in Figures 6 and 7 show the photoconductor response to various light intensities from which we obtain,

$$\tau = \frac{\sigma_s}{\Delta\sigma}\, t_L = \frac{\sigma_s}{\tan\delta} \quad \text{sec} \tag{15}$$

for this equilibrium lifetime the eq (15) only applies when $t_L > \tau > t_d$

and,

$$\tau_i = \frac{\Delta\sigma}{\eta K \phi - \frac{d(\Delta\sigma}{dt}} \quad \text{sec} \tag{16}$$

for which the light pulse duration $t_L \leq \tau$

From the same Figure 7 the quantum yield η may be calculated from,

$$\eta = \frac{2}{q\mu_2 K\sigma} \tan \phi_r \tag{17}$$

where ϕ_r is obtained from the initial risetime curve as depicted in Figure 7a and 7b.

The horizontal intercept with the risetime curve originates as shown in Figure 7b at tanh 1 = 0.76, with,

$$\frac{\Delta\sigma}{\sigma_s} = \tanh\frac{t_L}{2\tau} \tag{18}$$

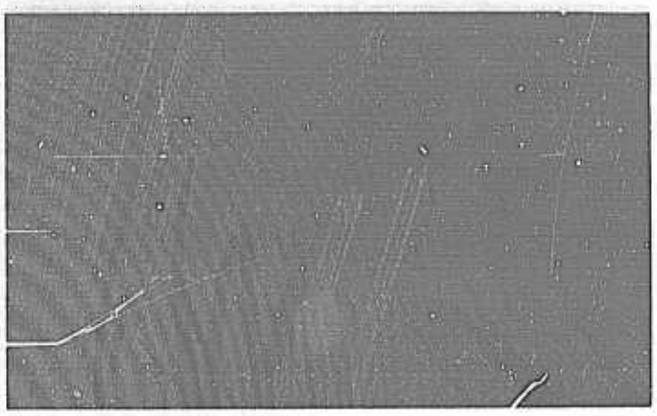

TYPE
9.05
9.02
9.00

(a) V 20 mv cm^{-1}
H 200 μ sec cm^{-1}
R_o 50 k Ω
L = 120 fcd

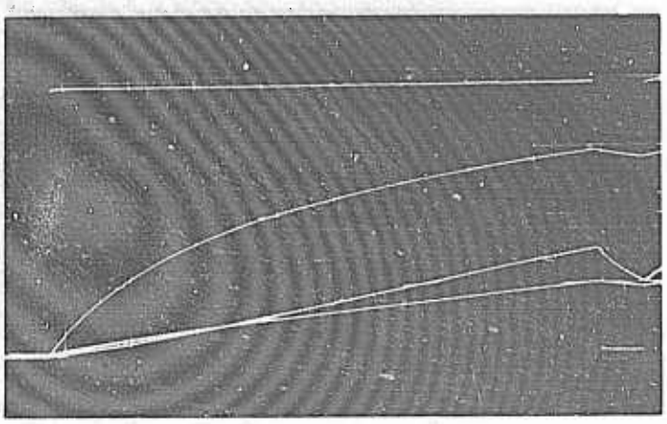

TYPE
9.02

(b) V 5 mv cm^{-1}
H 200 μ sec cm^{-1}
R_o 50 k Ω
L = 30 fcd

Figure 6

PHOTOCONDUCTOR RESPONSE TO LIGHT INTENSITY vs. TIME

(a)

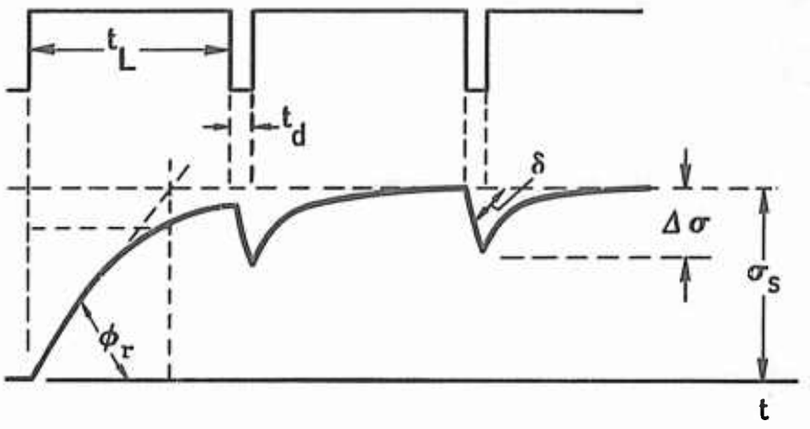

(b)

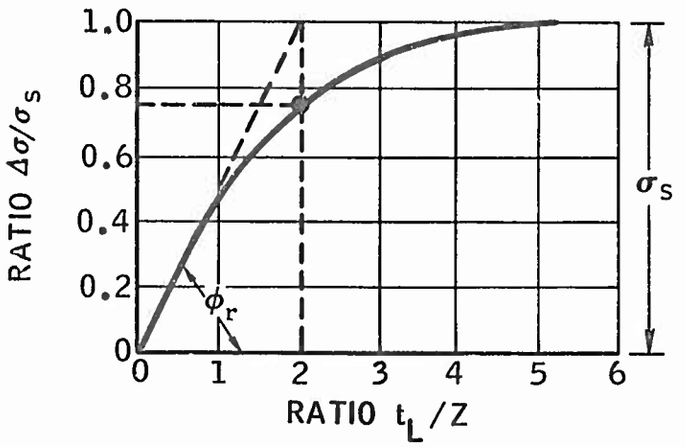

Figure 7

CONDUCTIVITY vs. PULSE TIME

hence eq (9) may also be written

$$\Delta\sigma = \sigma_s \tanh \frac{t_L}{2\tau} \tag{19}$$

The photon density ϕ satisfying the current requirement in eq (7) may be easily derived from the above set of equations describing the photoconductor performance.

Typical results for the photoconductor type 9.02 are shown in Figure 8 giving the conductivity vs illumination eq (10).

The conductivity vs voltage eq (8) is shown in Figure 9. This latter characteristic shows identical results between the type 9.02 and the type 9.05 graphically represented.

As shown in Figures 2 and 3 the addressing electroluminescent light bar covers the same area as the photoconductor with which, for all practical purposes, it is in optical contact.

What remains then is to define the energy transferred between photoconductor and electroluminescent cell. The brightness B to be achieved corresponding to the desired photons flux ϕ satisfying the switching time t_s, follows from,

$$\phi = \frac{C}{hc} \int \lambda \frac{dE}{d\lambda} \, d\lambda \tag{20}$$

$$= 5\ 10^{15}\ CQ$$

$$\text{with } Q = \int \lambda \frac{dE}{d} \, d\lambda \quad \text{number of integrated quanta} \tag{21}$$

where the constant C takes into account the units used for spectral energy and the unit of measurement in watts cm^{-2}.

With the units 685 lumens $watt^{-1}$ and square foot - 924 cm^2

$$B\ ft\ L = \frac{685 \times 924\ C}{A_2 cm^2} \int y \frac{dE}{d\lambda} \, d\lambda$$

$$= \frac{685 \times 924\ CL}{A_2}$$

with L a luminosity factor accounting for mismatch between the electroluminescent light spectrum and the eye response.

with $hc = 1.98\ 10^{-23}$ watt sec^{-1}

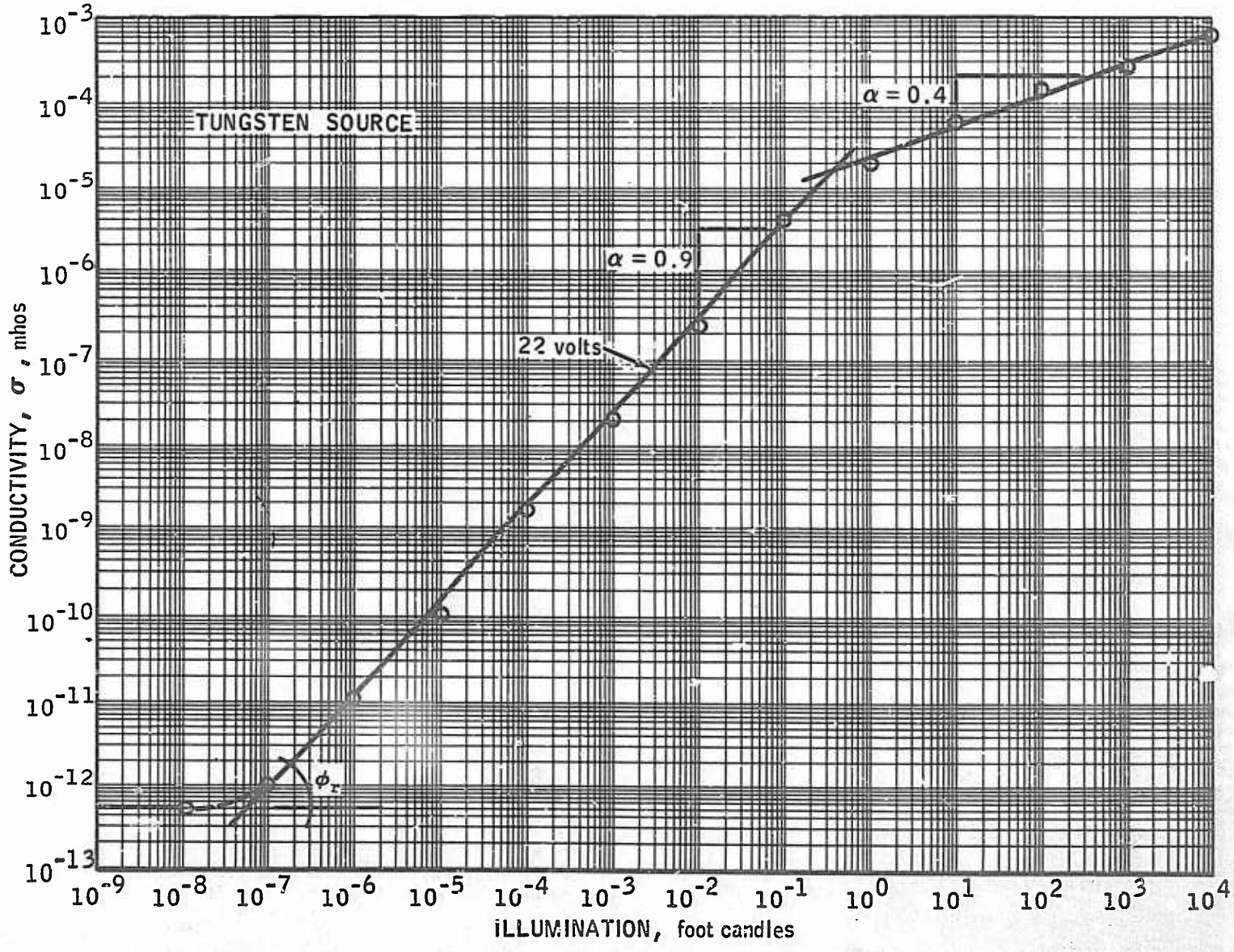

Figure 8

CONDUCTIVITY AS A FUNCTION OF ILLUMINATION (RUN NO. 9.02)

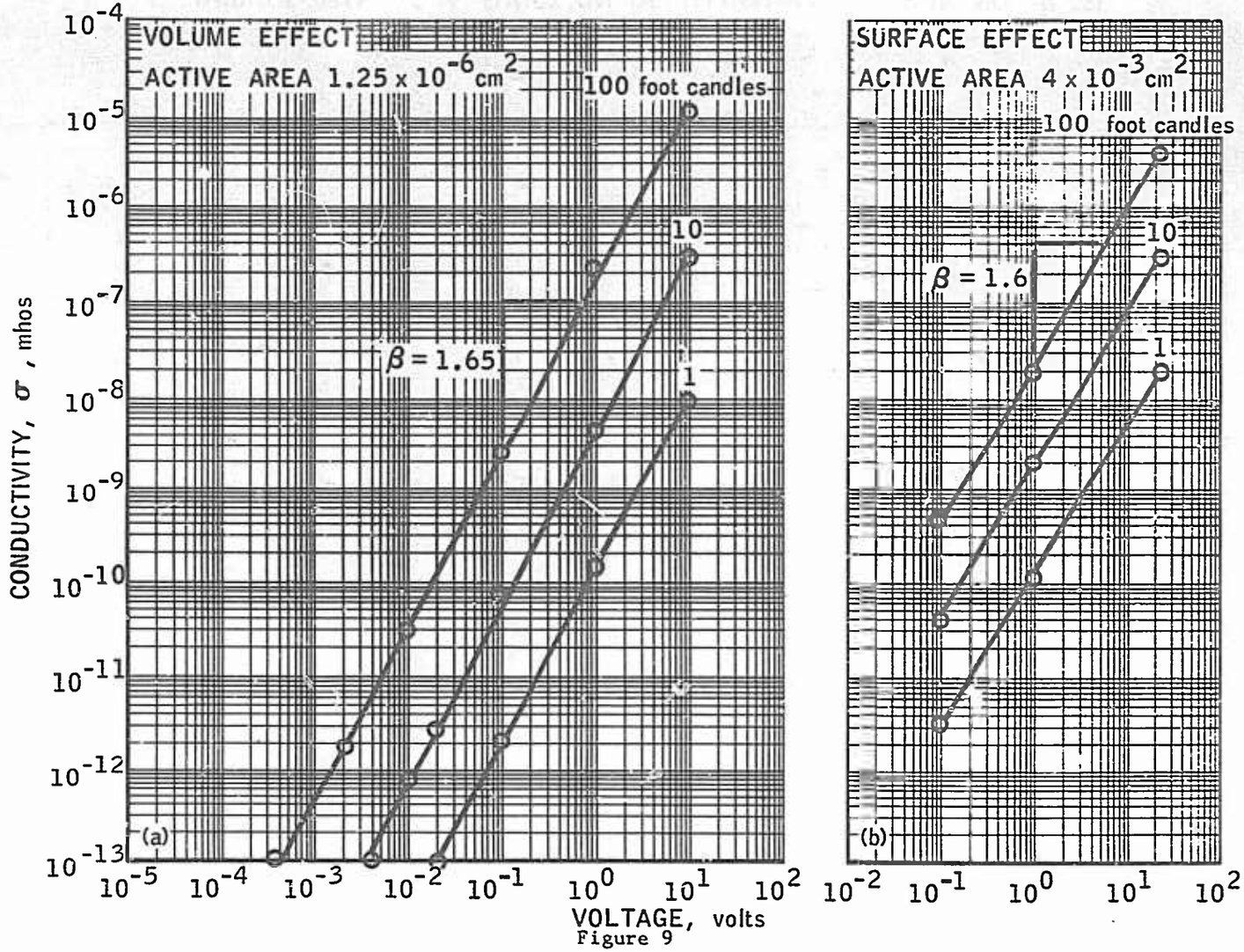

Figure 9

PHOTOCONDUCTOR CONDUCTIVITY vs. VOLTAGE
(RUN NO. 9.05)

$$\frac{Q}{1.9810^{-23}} \qquad \frac{AB}{685 \times 924L}$$

$$\phi = \frac{BAQ \times 8 \times 10^{16}}{L} \tag{22}$$

From Figures 10 and 11 it can be seen that a very close match is achieved between photoconductor #9.02 spectral response and the light spectrum emitted by the electroluminescent cell; both have their maximum response at approximately 6000 Å.

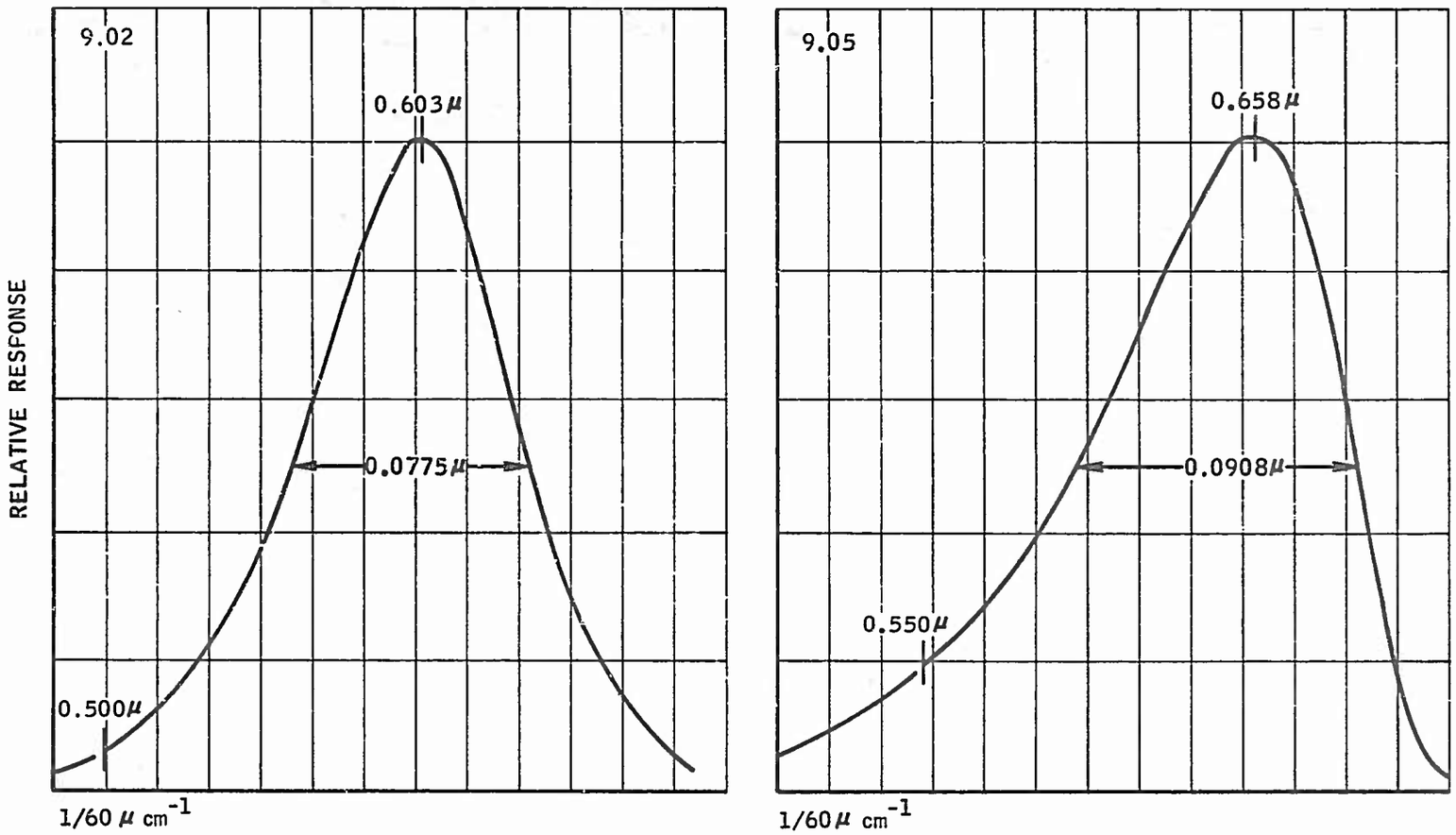

Figure 10

PHOTOCONDUCTOR SPECTRAL RESPONSE

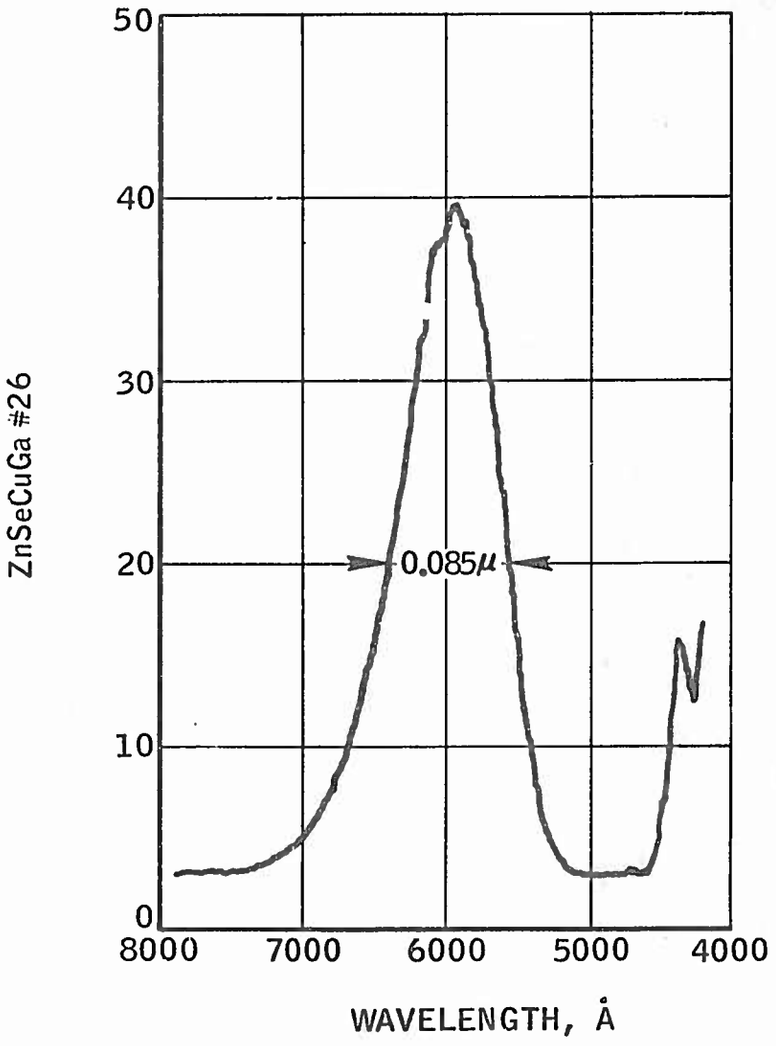

Figure 11

pin DIODE ZnSeGa SPECTRAL EMISSION

SECTION III

EXPERIMENTAL ELECTROLUMINESCENT WORK

1. BACKGROUND

The production of II-VI compounds in large monocrystals from the liquid phase is made difficult by the high vapor pressure of the elements at their melting point. (1) (2)

In the compounds of interest viz ZnTe and ZnSe, the high temperature of formation (3) (4) imposes severe limitations on crucibles and containers usable for their growth (5) (6). An alternative method used by growing the crystals from the vapor phase (7) (8) yields small crystals often presenting numerous dislocations and inclusions.

Since the thickness of any part of a junction is by necessity comparatively small, the epitaxial growth over large areas is obviously a tempting solution. The work published to date on epitaxial deposition is scarce and generally involves a substrate of identical species. (9) In this particular reference one of the crystalline compound is used as a substrate for epitaxing the other component from its vapor: this leaves the problem of area unresolved. ZnTe has been deposited epitaxially from the vapor in vacuum (10) on LiF and CaF_2, but films so produced are said to peel easily from their substrates.

2. SUBSTRATES PREPARATION

Two types of substrate were extensively used during this work; CaF_2 crystals purchased from Isomet Corporation, Palisades Park, New Jersey, and αAl_2O_3 purchased from Union Carbide Corporation, Electronic Division, Torrance, California.

The same cleaning procedure was applied to all crystals prior to and after etching. The substrates were ultrasonically cleaned in Triton 100X, for 5 minutes, rinsed several times in deionized water, followed by alcohol rinse and forced air drying.

The CaF_2 crystals 1" x 1" x 0.25" were cleaved to around 0.040" thickness and etched in H_3PO_4 heated at 165°C. The <111> etch pattern obtained after 20 minutes is shown in Figure 12. The CaF_2 crystals are very sensitive to thermal shock and great care had to be exercised in order to avoid shattering of the platelets. After cleaning the etched crystals and a careful rinse in water and alcohol, the substrates were immediately transferred to the vacuum chamber.

Two types of flame fusion sapphire crystals were purchased, 1" x 1" x 0.040" and disks of 0.5" diameter, 0.015" thick. They were respectively oriented in <11$\bar{2}$0> plane and for the disks in <0001> plane.

Occasional fine scratches remaining from the diamond powder polish were still visible under high magnification.

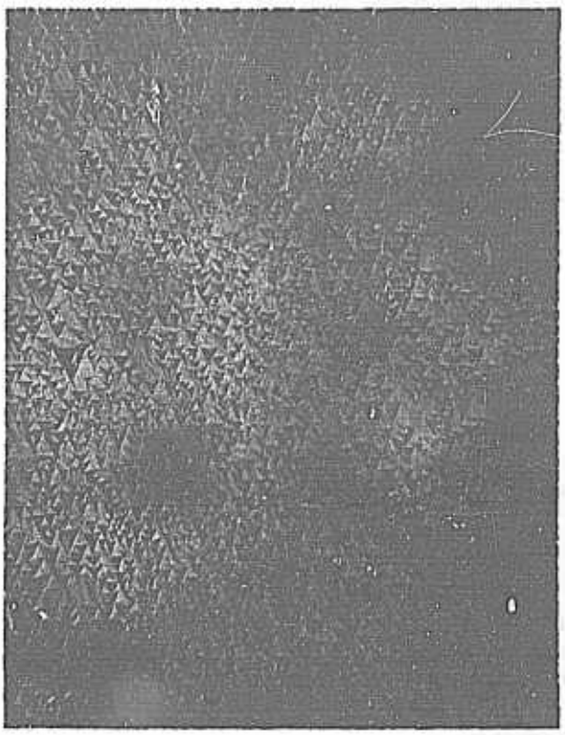

100X

Figure 12

ETCHED CALCIUM FLUORIDE
<111>

No etching was attempted on the $<11\bar{2}0>$ cut crystals, while the $<0001>$ were thermally etched in a fluorinated hydrocarbon vapor. (11)

The disks were placed on a carbon susceptor and introduced in a Vycor tube 1" I.D. The Vycor tube was fitted in a tubular furnace, well ventilated and heated progressively to 950°C, under a small flow of dry argon. When thermal equilibrium was achieved, a flow of 5 ml min^{-1} of $C_2Cl_2F_4$ (Freon 114), from the Matheson Co., was introduced and the flow of argon cut off. After cooling to room temperature, the cleaning procedure was again applied to the disks, prior to their introduction in the vacuum chamber.

A 35 minute etch pattern of the $<0001>$ cut is shown in Figure 13.

3. VACUUM EQUIPMENT

The vacuum system comprised a six inch diffusion pump with a double baffle, one water cooled the other cooled with liquid nitrogen.

Two additional pumps were attached to the 18" metallic bell jar, both from Varian Associates, one a titanium sublimation pump and the other an 18 liters ion pump. A Veeco mass spectrometer was mounted on the side of the bell jar with a high vacuum isolation valve of large aperture. The axis of the mass spectrometer made an angle of 30°, with the normal to the coaxial gap of the evaporating sources, Figure 14.

After degassing the system for 8 to 10 hours at 150°C, the residual pressure, measured with a nude ion gauge, never exceeded 10^{-8} torrs in the vacuum enclosure prior to each evaporation, Figure 15.

Besides N_2 and CO_2, which are the main contributors to the background pressure, the residual gases consist mostly of the dienes C_3H_3, from cracking of the Corning 702 silicon oil. Figure 16 represents the mass and magnitude of the residue measured at 10^{-8} torrs after thorough degassing.

The sources used for evaporation have been developed under NASA Contract NAS 12-545, February 1968, the details of which are shown in Figures 17 to 19.

The source shown comprises 2 concentric troughs, the inner one evaporating zinc the outer one the chalcogene. The two troughs are at different temperatures, each independently controlled by separate radiative heaters, the outer one made of tantalum, the inner one of carbon.

The partition between the two troughs is made of such thickness that the temperature differential between the faces in contact with metal and chalcogene is around 85°C.

Both elements mix their vapors in the circular evaporating gap, whose cross section represents a circular evaporating source. The width of the gap in this Knudsen source is a very small fraction of the molecules mean free path at any operating pressure used.

Just below the gap opening in the chalcogene trough a coaxial thoriated tungsten filament is suspended by two diametrically opposed points which feed the current in the loop.

200X

Figure 13

ETCHED SAPPHIRE
<0001>

R-26,918

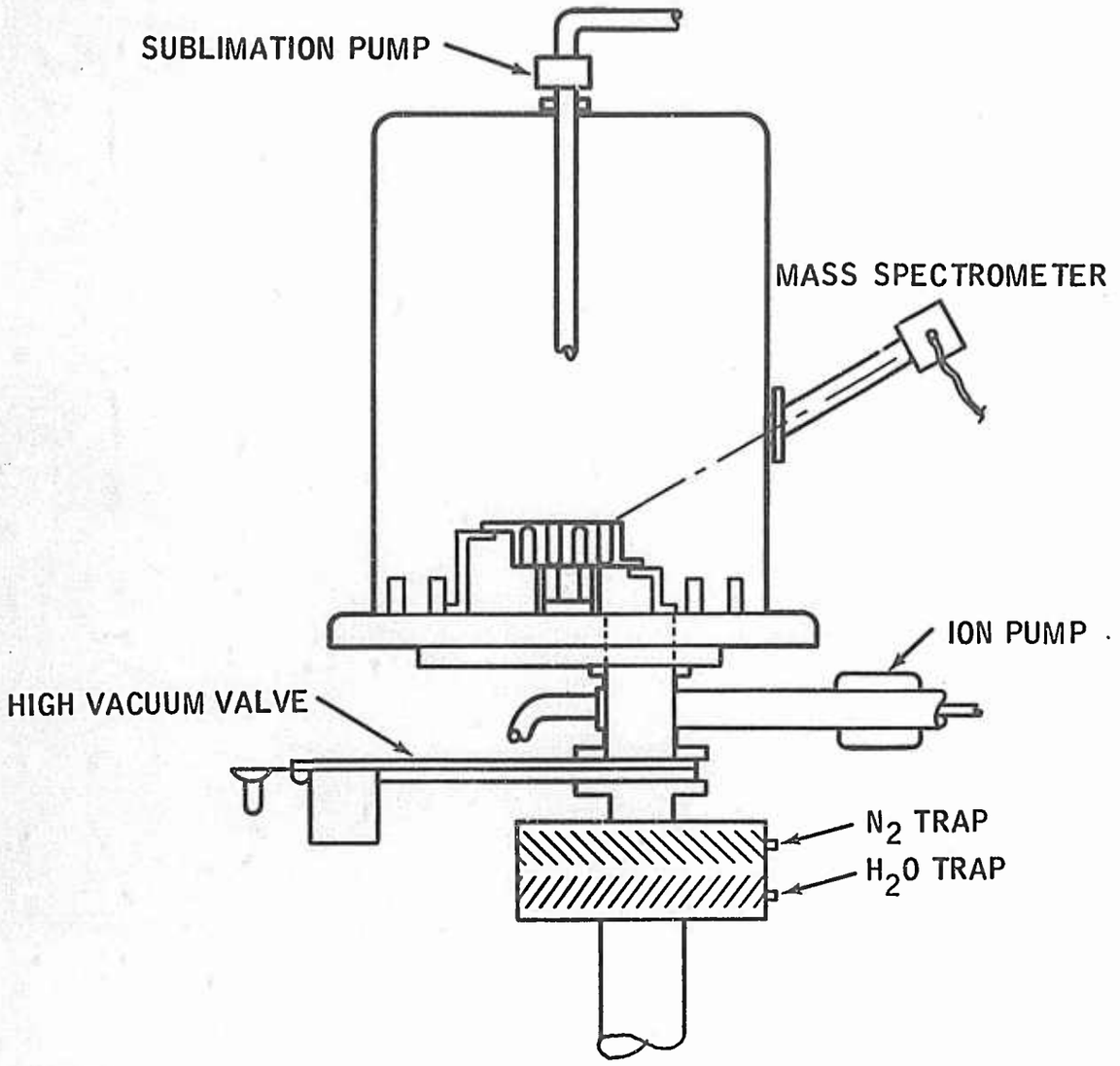

Figure 14

VACUUM SYSTEM

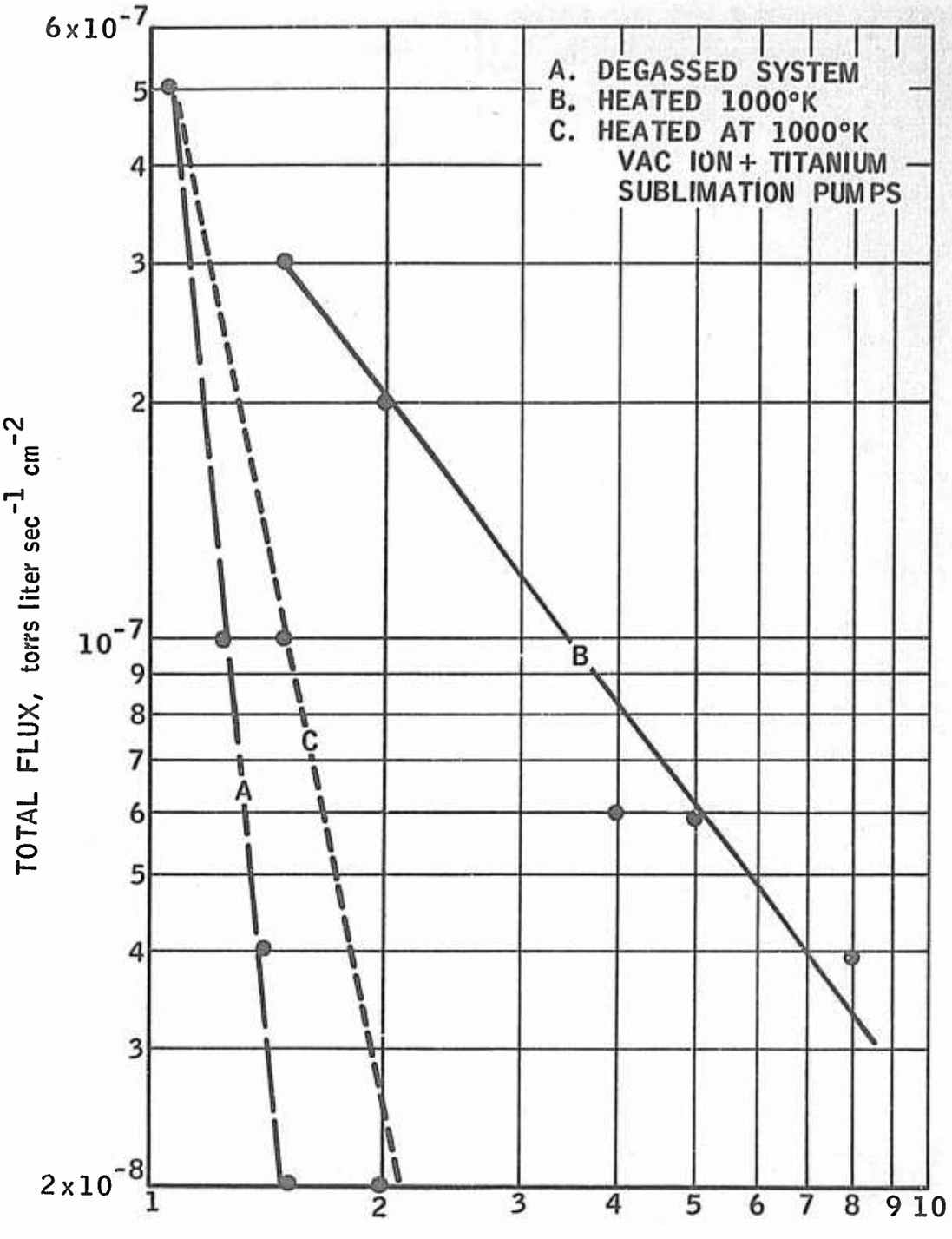

Figure 15

PRESSURE vs. PUMPING TIME
AND SYSTEM CONFIGURATIONS

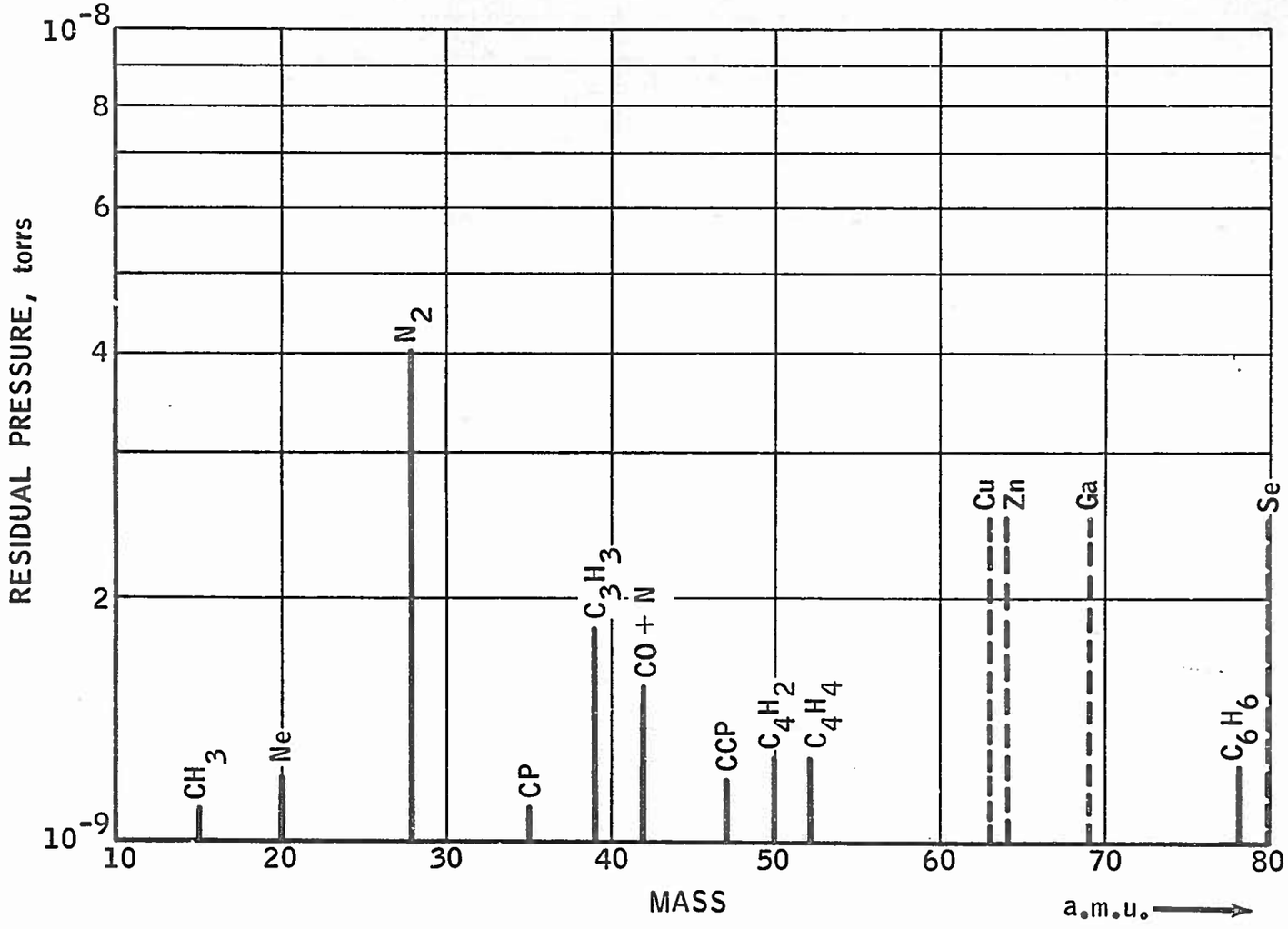

Figure 16

MASS SPECTROGRAPHIC ANALYSIS OF RESIDUALS

R-23,910
Neg. 8716-2

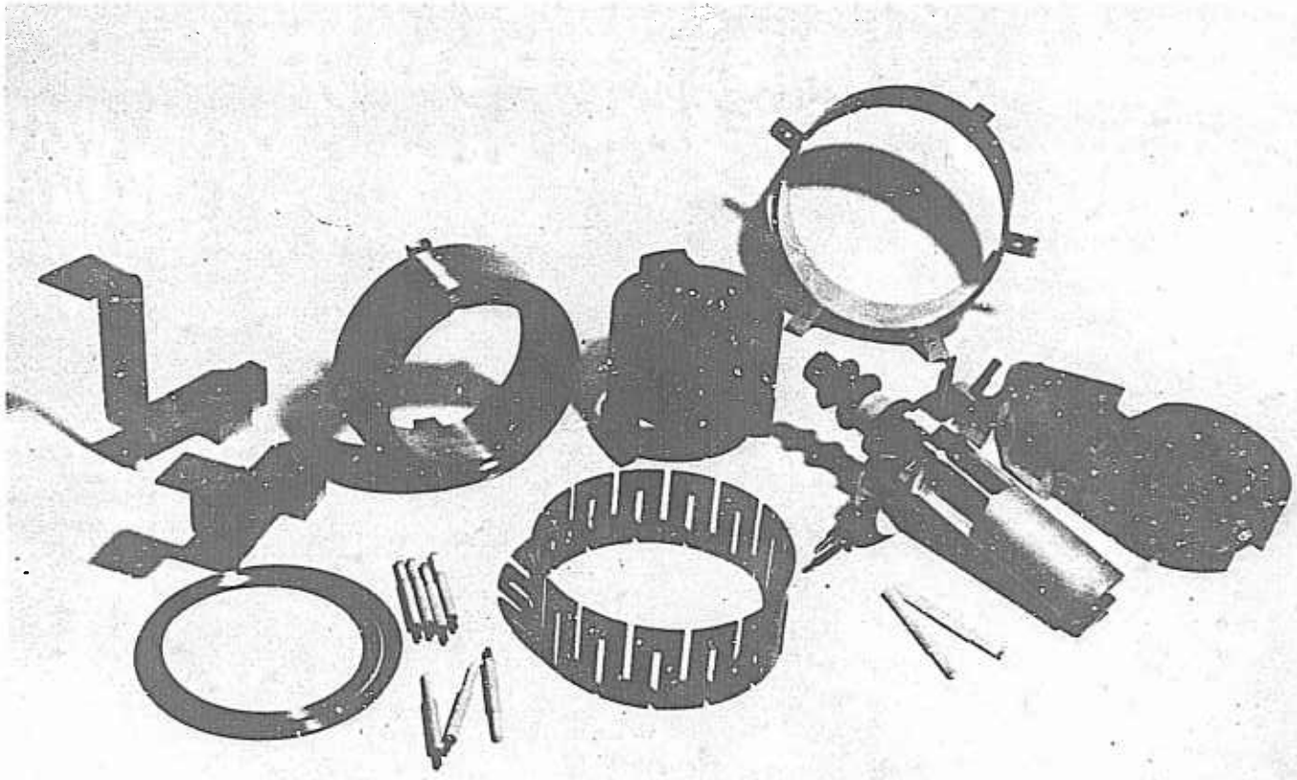

Figure 17

COMPONENTS OF EVAPORATOR SOURCE CONFIGURATION

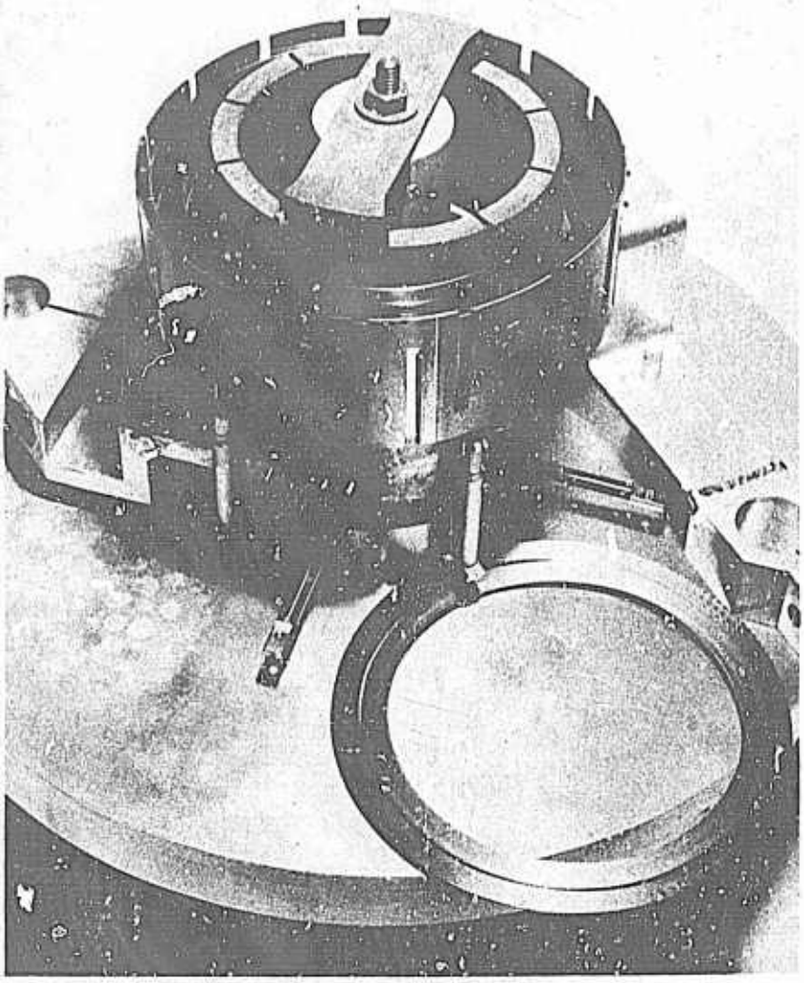

Figure 18

ASSEMBLED EVAPORATOR SOURCE CONFIGURATION

R-23,909
Neg. 8716-1

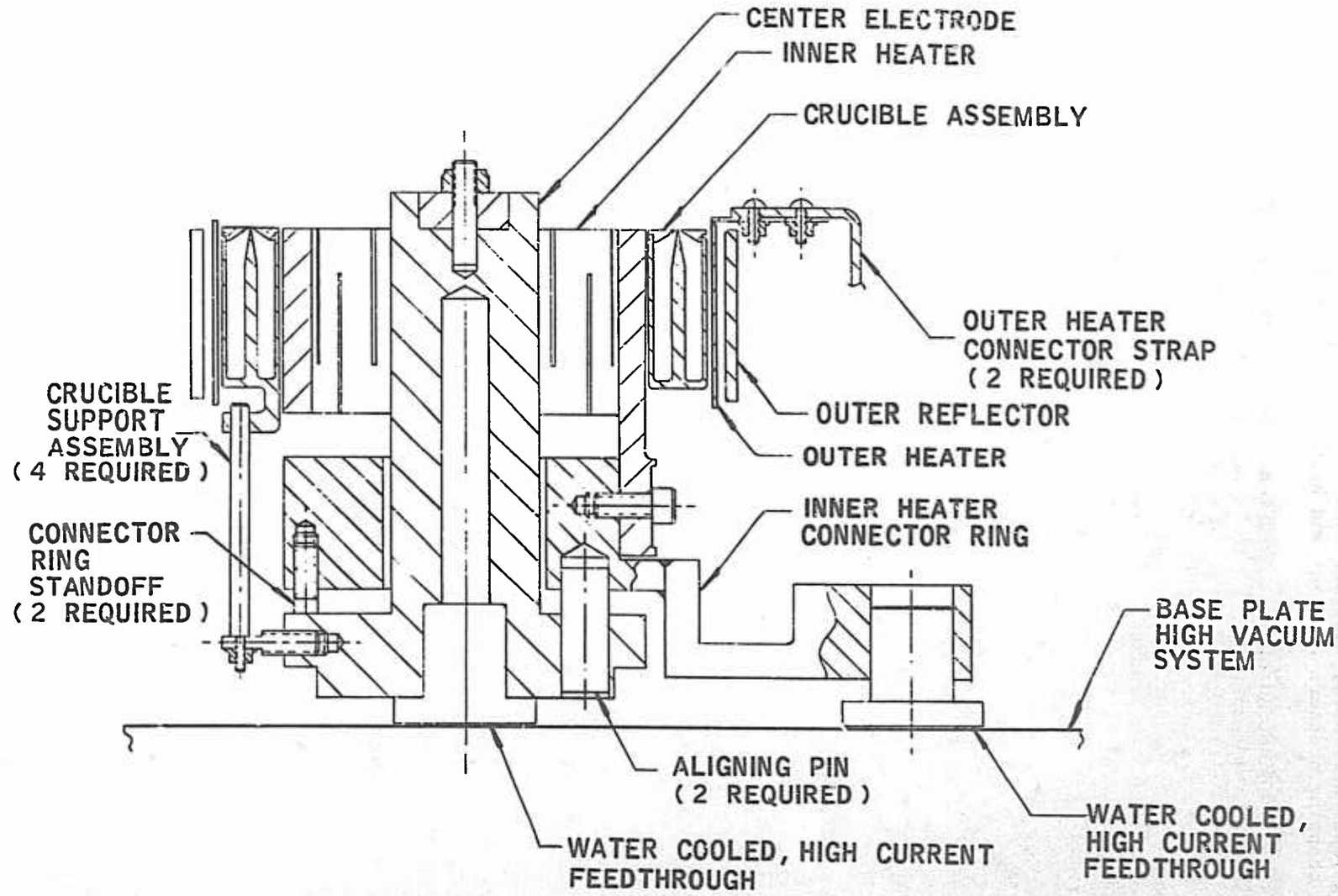

Figure 19

EVAPORATION HEATER SOURCE

Initially the filament was brought at a temperature in excess of 2000°C and the energy radiated shattered the high order polymer. The control of the evolving vapor presented, however, some difficulties with this approach, due to fast changing pressure gradient and high residual of dimeric specie.

Ultimately, instead of thermally ionizing the evolving chalcogene up to around 3000°K, the temperature of the concentric filament was lowered to about 200° above the melt's temperature. A potential of approximately 300 volts was applied between the thin thoriated tungsten filament and the wall of the Se crucible. The diode current was adjusted between 200 to 300 milliamps. This collision approach in breaking the atomic clusters of the chalcogene polymers[1] has shown the evolving vapor to be essentially monomeric, Figure 20.

The actual discrepancy observable between the isotopes amplitude of mass 78 and 80 of Se comes from the residual pressure of C_6H_6 of benzene shown in Figure 20.

The output of PtRh and ion-constantan thermocouples attached to sources and substrate heater controlled the respective temperatures to within $\pm$ 1°C. A good thermal contact was assured between substrates and heater, the drop in temperature due to substrate thermal conductivity was accounted for.

4. VAPOR DEPOSITION

Thermodynamic third law method was applied in calculating total and partial pressures from,

$$\log K_p = \frac{\Delta fef + \frac{\Delta H298}{T}}{4.576} \qquad (23)$$

where

$$P = pZnSe + p\ Zn + pSe$$

The calculations are summarized in Figures 21 and 22, which show the vapor pressure of the elements and the equilibrium pressure of the compounds ZnSe and ZnTe.

Since the main interest is actually directed towards ZnSe, only the results for this compound are summarized in Figure 21, representing the molecular concentration of specie at a source temperature T, as $\eta_i = f(T)$, from the relation,

$$\eta_i = \frac{P_i}{(2\pi m_i\ kT)^{\frac{1}{2}}} \quad cm^{-2}\ sec^{-1} \qquad (24)$$

It is seen that the molecular concentration from the evaporating compound is far below the values of any of the two components.

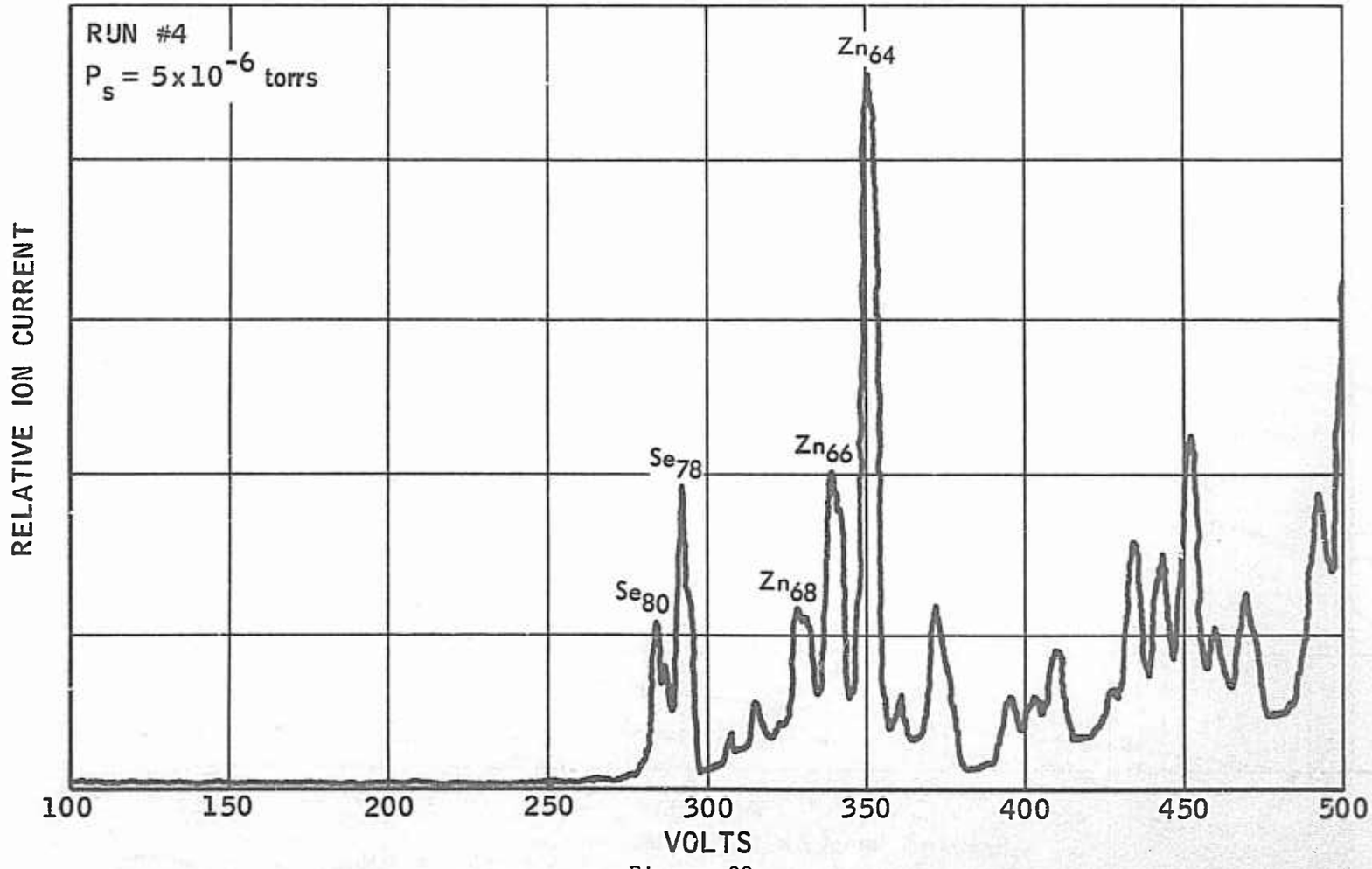

Figure 20

MASS SPECTROGRAPHY OF COEVAPORATED Zn + Se
CONCENTRIC TMC SOURCES. THERMAL IONIZER.

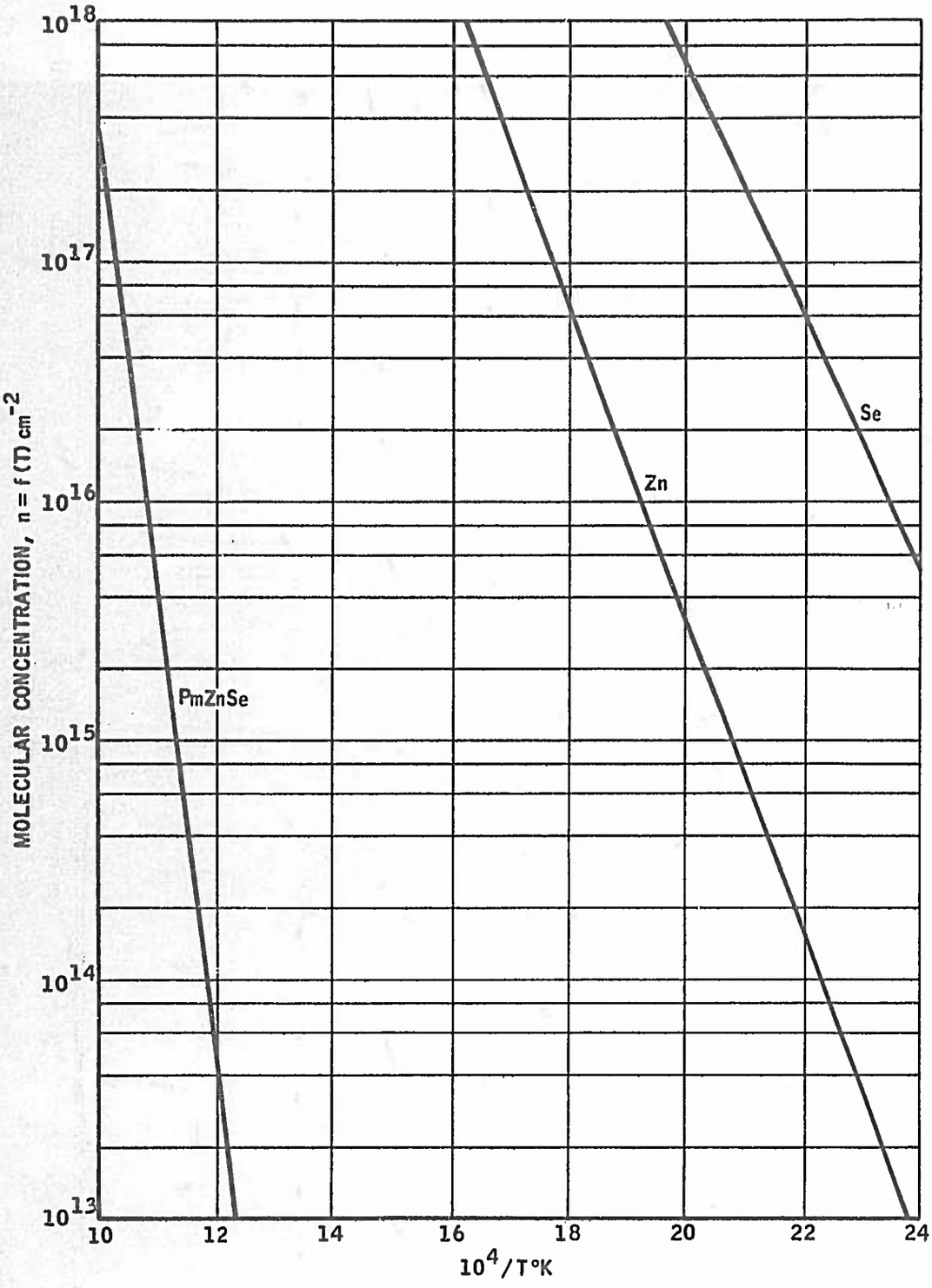

Figure 21

EQUILIBRIUM CONCENTRATION

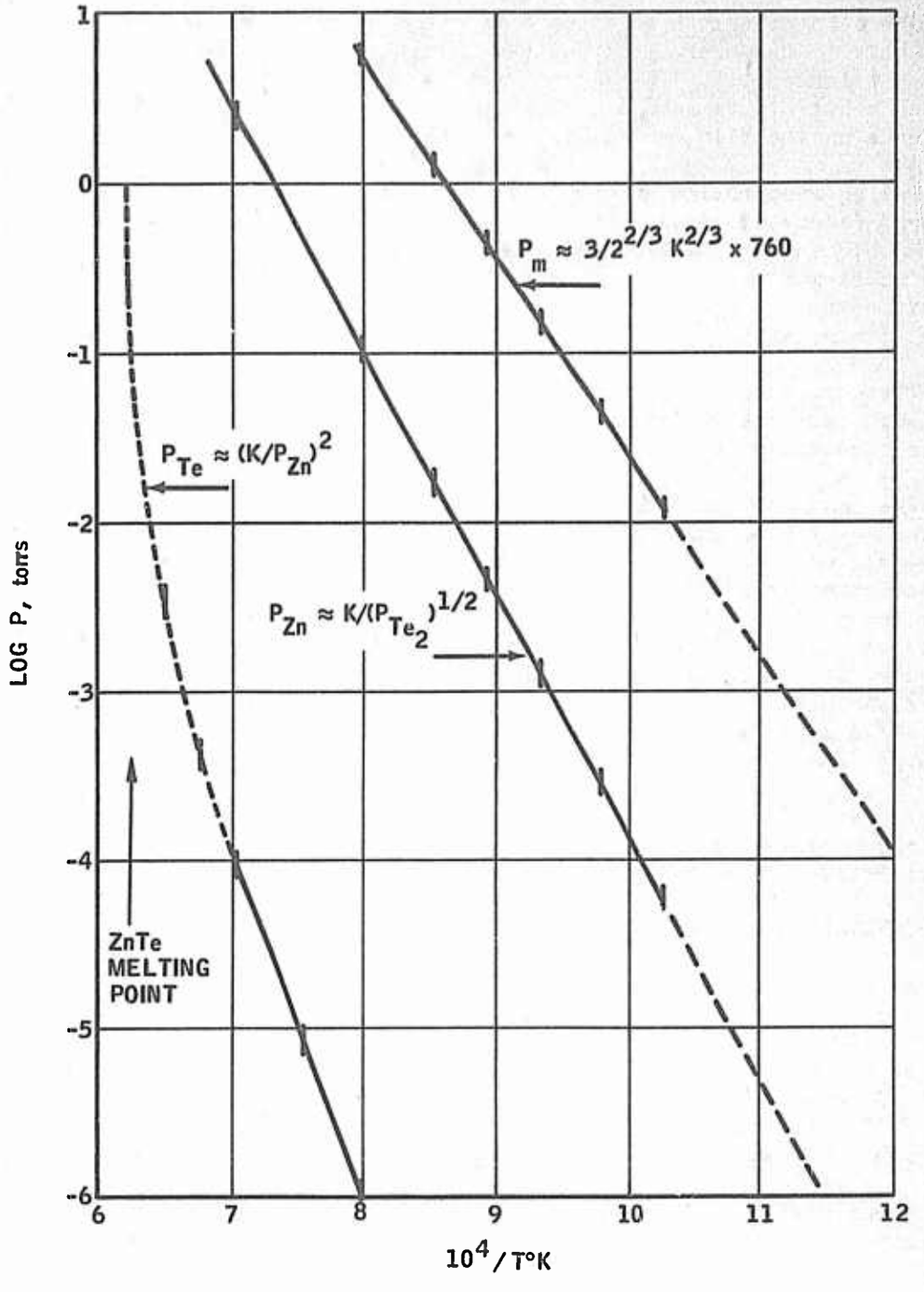

Figure 22

VAPOR PRESSURES OF VAPORIZING ZnTe

Present nucleation theories do not permit a straightforward approach in calculating condensation parameters for binary vapors. Actually a purely experimental approach was followed in evaluating the epitaxial deposition of ZnSe and ZnTe.

The main object of this phase of the work was first to assess the role of the substrate temperature versus the molecular concentration (eq 24) on the film's stoichiometry. The second step was to investigate the interdependence between substrate temperature, molecular concentration, and angle of vapor incidence on the film crystallization.

During evaporation of any II-VI compounds, dissociation occurs and the compound reconstitutes itself during condensation by chemical association between elements. The same thing occurs when the compound formation proceeds from the elements. It is well established that this occurs even when the condensation temperature is well above the critical condensation temperature of the elements, irrespective of the vapor concentrations.

The current procedure adopted in this work was to keep one source at a constant pressure, while the other was used as the variable for each new setting of substrate temperature.

The condensation rate of the ZnSe compound is shown in Figure 23 on which stoichiometric range has been plotted. Each film was evaluated for composition by X-ray fluoroscopy. The results of these measurements are shown in Figure 24. The deviation from stoichiometry is shown to increase rapidly as a function of vapor composition. The large ratio Se/Zn accounts for several conditions, first, the lower critical condensation temperature for Se compared to Zn. Secondly, it was observed that a higher Se content in the impinging vapors favors one particular crystalline structure. The density of trapping centers in II-VI compounds is structure sensitive and was found to increase with increasing contribution from mixed crystalline phases.

It can be seen from these measurements that stoichiometry occurs only in a fairly narrow range of vapor concentrations for any condensation temperature experimented with.

5. CRYSTALLINE STRUCTURE

Both ZnSe and ZnTe are known to have polymorph structures, i.e., they both can occur in cubic and hexagonal phases. (12) (13)

As a guide to structure identification, the position of the main planes of a ZnSe crystal are indicated as a function of the refracting angle in Figure 25. In these figures the respective reflection intensities are shown for both cubic and hexagonal planes.

Along with the crystal plane identification, the procedure involved an evaluation of the degree of crystallization of the films correlated with processing parameters.

Plane spacings in Debye Scherrer photographs were calculated by Straumanis method; in these, or in diffractometer recordings, the Cu K α wavelength(14)

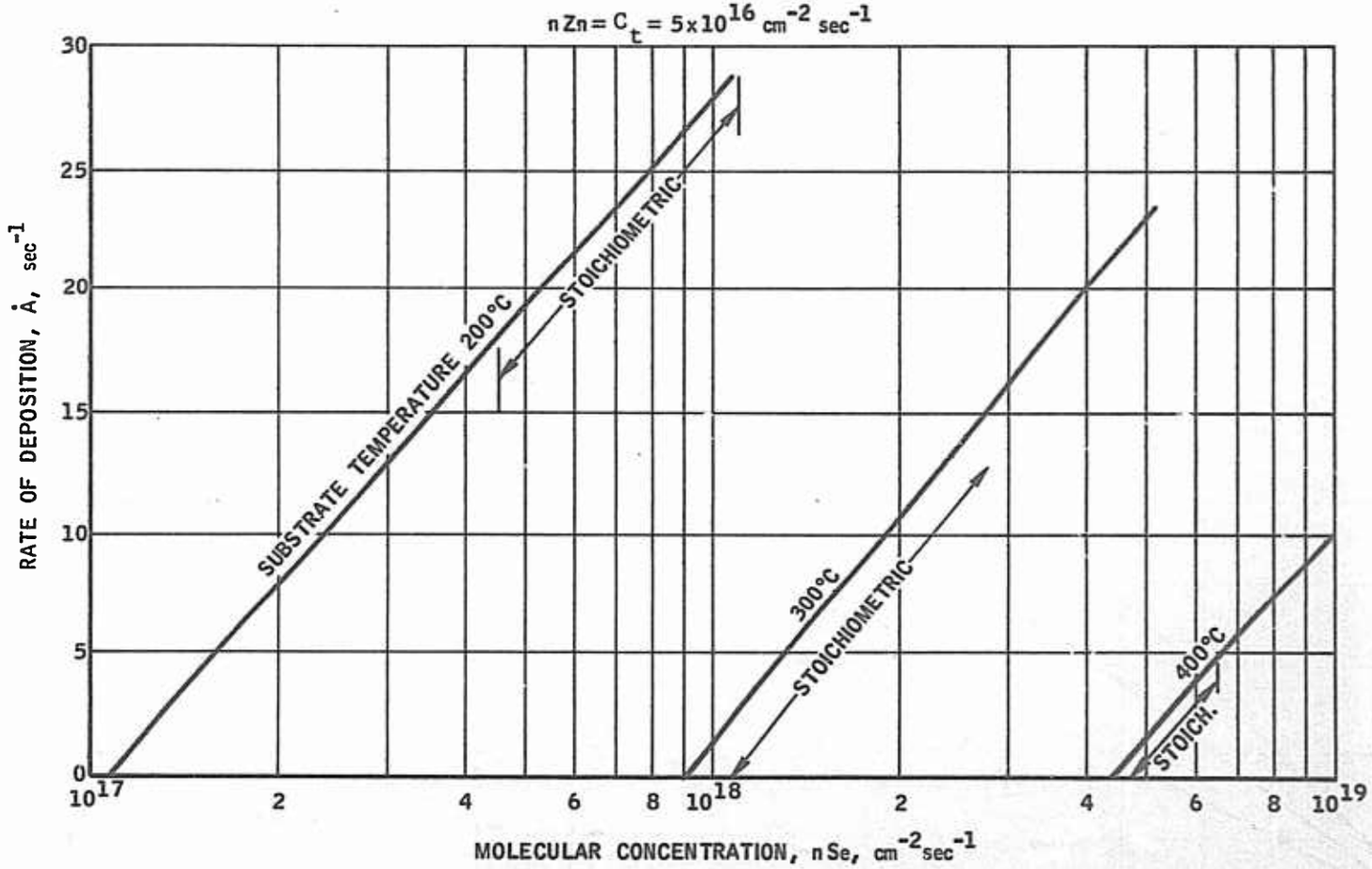

Figure 23

GROWTH OF ZnSe LAYER FUNCTION OF MOLECULAR FLUXES

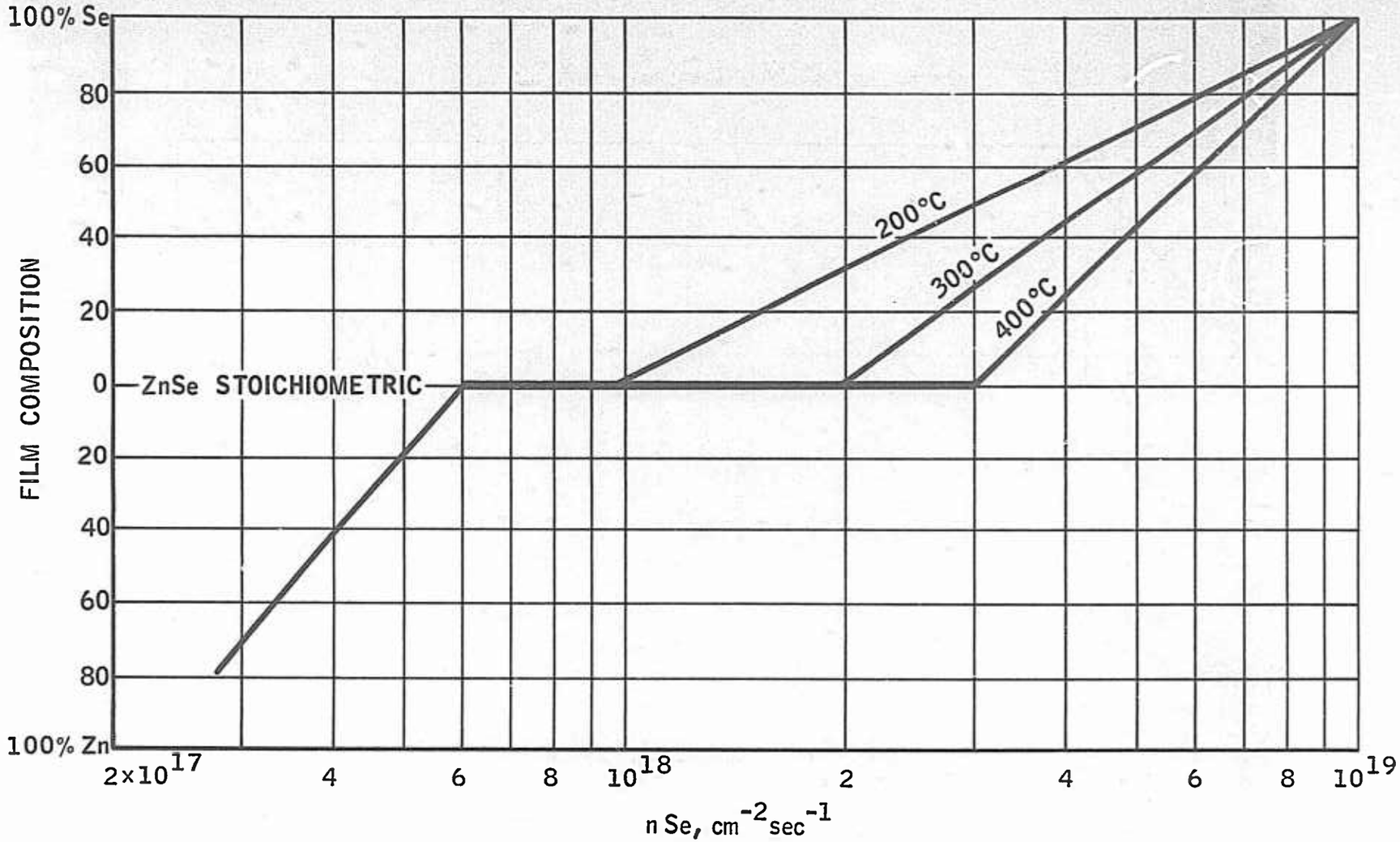

Figure 24

FILM COMPOSITION vs. Se FLUX AT Zn FLUX CONSTANT

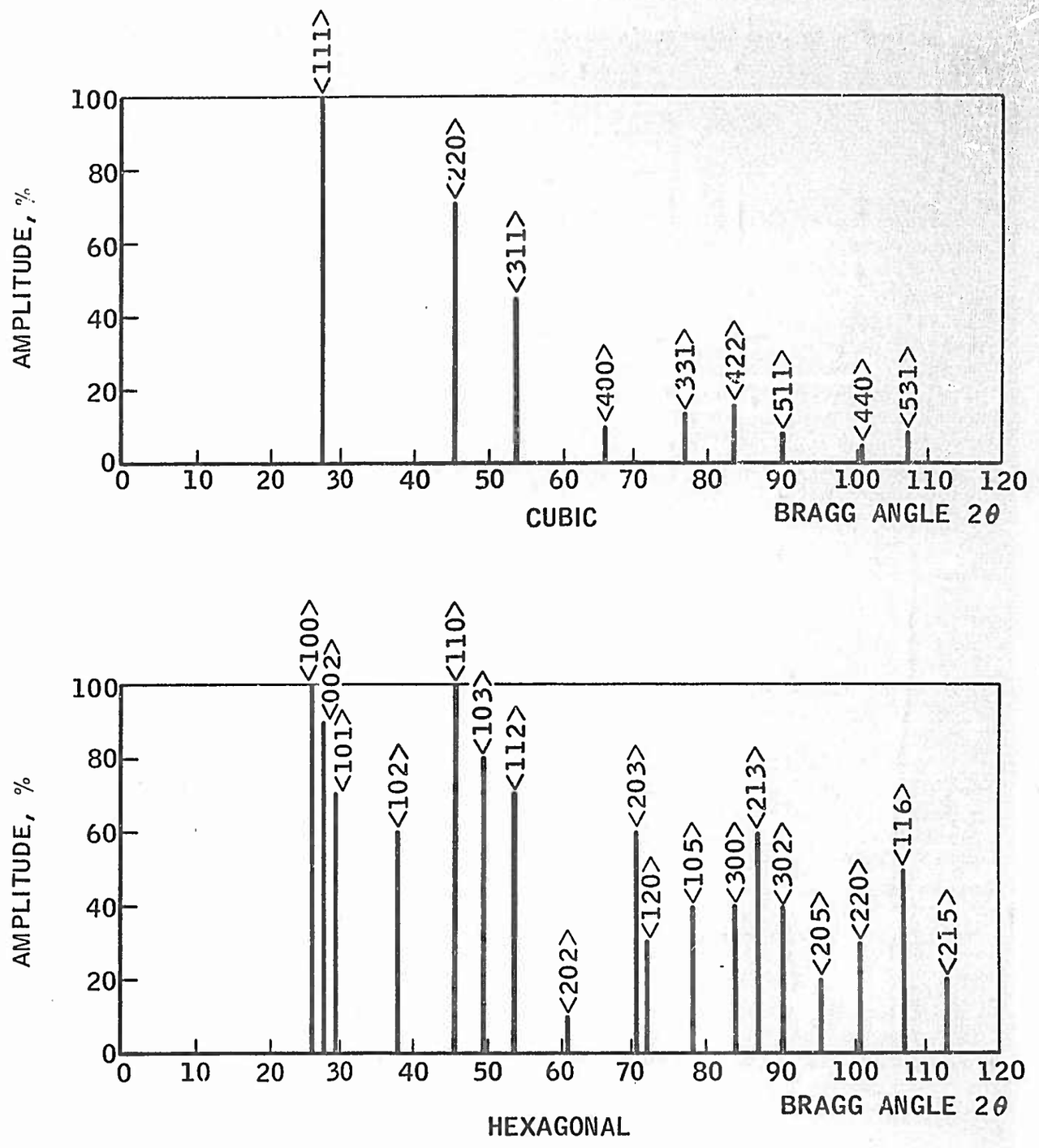

Figure 25

ZINC SELENIDE DIFFRACTION PATTERNS

was used throughout. The diffraction patterns for ZnSe and ZnTe are shown in Figures 26 and 27 respectively. In back reflections, calculation of position and indices of Laue spots was made from the Kedesy method.[15]

Attempts to use Scherrer's equation for crystalline size determination, from,[16]

$$D = \frac{0.9\,\lambda}{\beta \cos\theta}$$

(θ Bragg angle; β half breath; λ = CuK α) proved to be too cumbersome to manipulate in most cases. A simpler, though qualitative method[17] was used instead.

On back reflection Laue photographs, a parameter R defines the degree of crystallization; it is given the value 0 for patterns showing only diffused rings; a value of 25 is assigned to R for mixed rings and spots patterns, in which the ring aspect predominates; 50 for R indicates that spots and rings have identical intensities; 75 is assigned to mixed patterns where the spots predominate; finally R is equal 100 for spots pattern only.

The slope of the straight line describing R = f (T) was obtained from least square method, from,

$$\frac{Y_R}{X_T} = \frac{n\,\Sigma xy - \Sigma x\,\Sigma y}{n\,\Sigma x^2 - \left(\Sigma x\right)^2}$$

with n the number of experimental points. A graphical representation of this function is given in Figure 28 in (a) for ZnSe and in (b) for ZnTe.

Back reflection Laue spots from perfect crystals are sharp. While arcing of the spot reveals that the deposit contains nuclei rotated about the normal to the specimen plane. Fine rings indicate a well defined structure but made up of small crystallites. The Laue photographs shown in Figures 29 to 32 illustrate the various steps in the process for ZnSe and in Figures 33 to 34 for ZnTe.

Figure 29 (a) corresponds to a substrate temperature of 150° and 250° for (b).

Figure 30 (c) and (d) were obtained for an identical substrate temperature but at different incident nZn, they show clearly varying contribution of the hexagonal phase.

Figure 31 (e) shows the reflection produced by the <0001> sapphire with a film of ZnSe of thickness around 1500A.

(f) shows an increased organization in the nuclei towards a cubic structure although the hexagonal contribution is still significant.

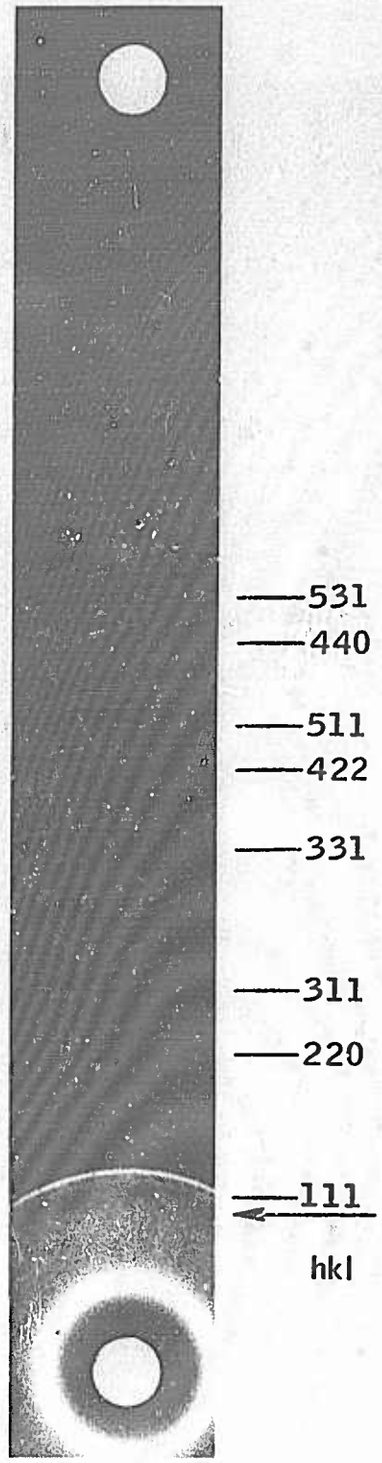

Figure 26

ZnSe DIFFRACTION PATTERN
RUN #4

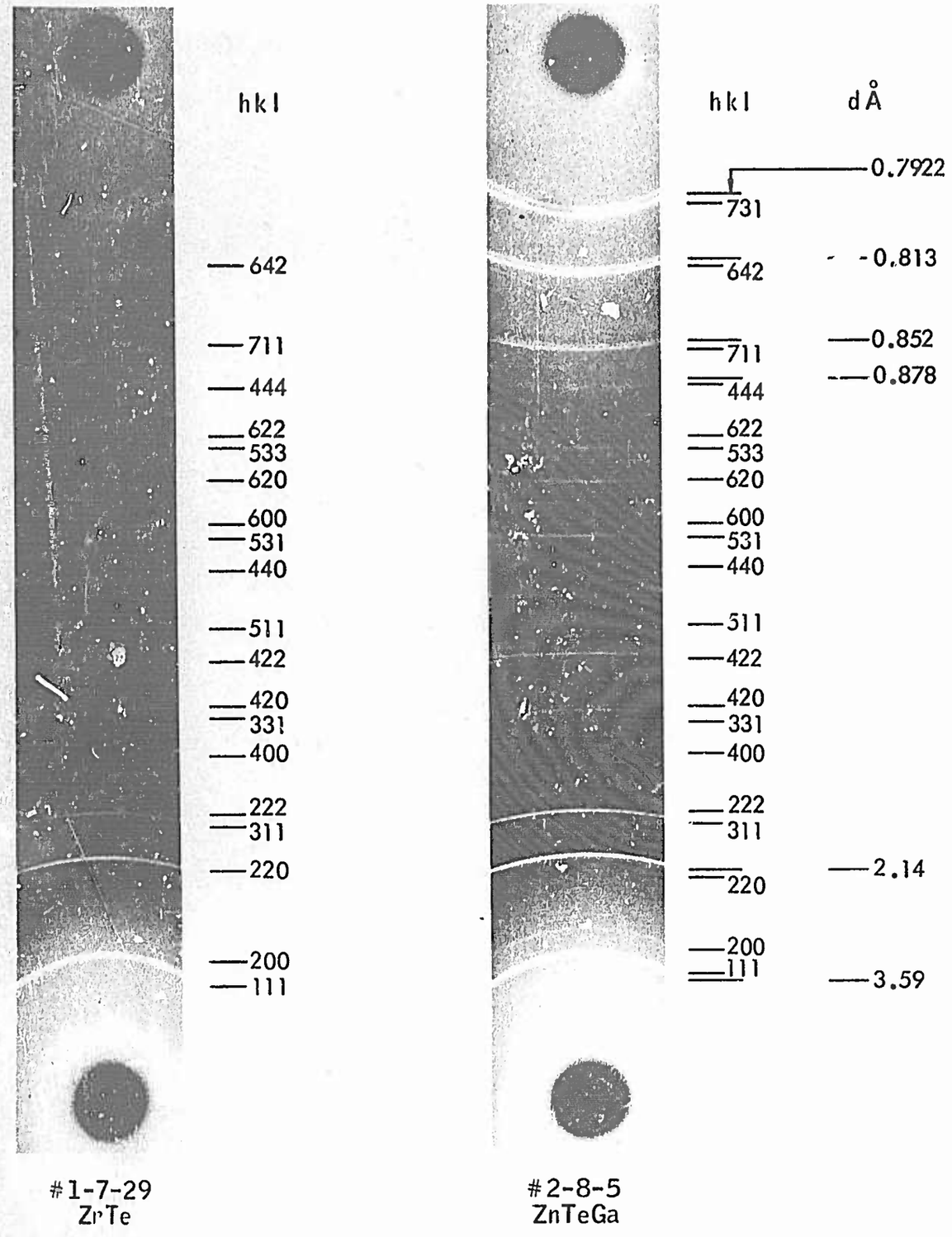

Figure 27

ZnTe DIFFRACTION PATTERN

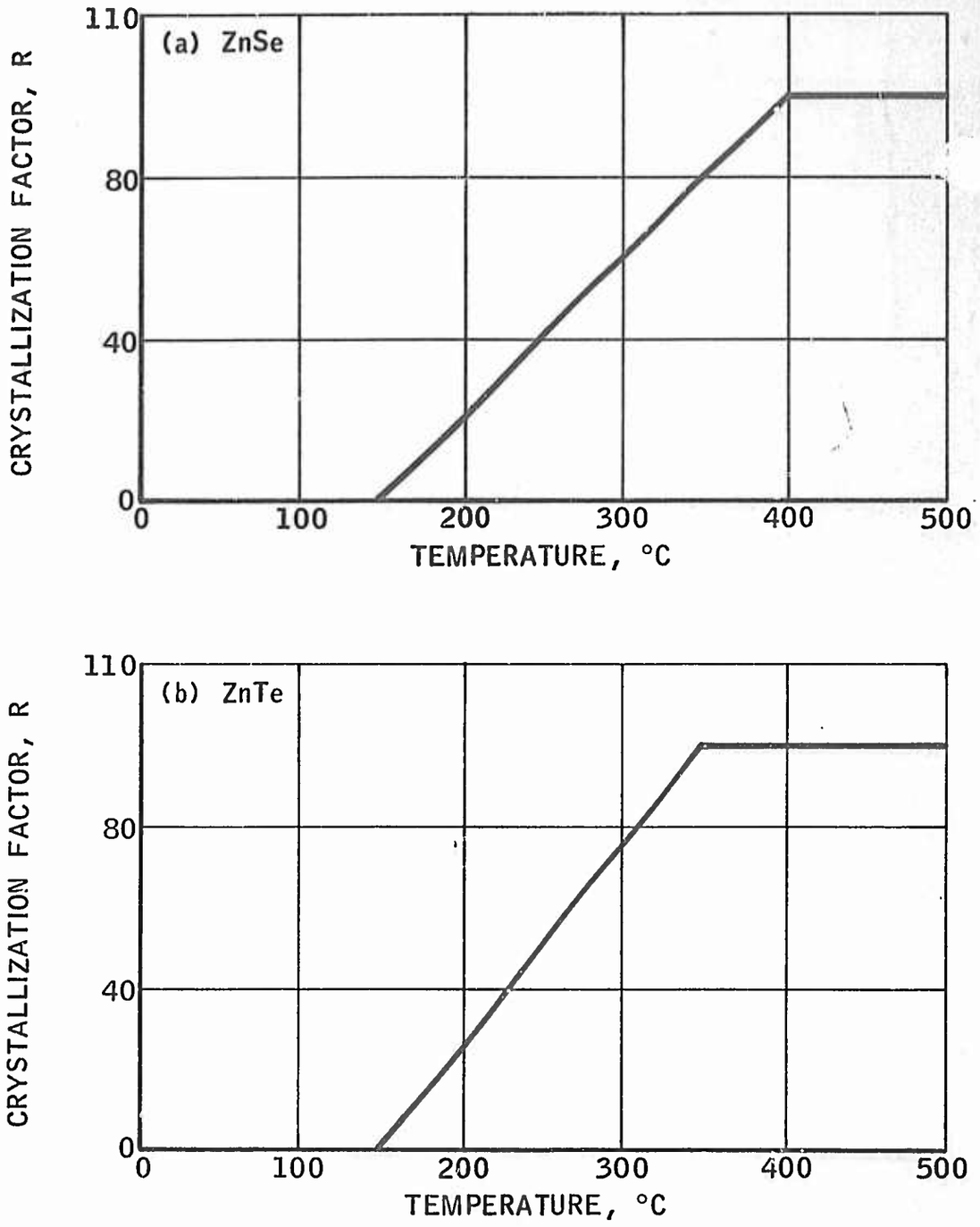

Figure 28

EPITAXIAL GROWTH ON <0001> SAPPHIRE

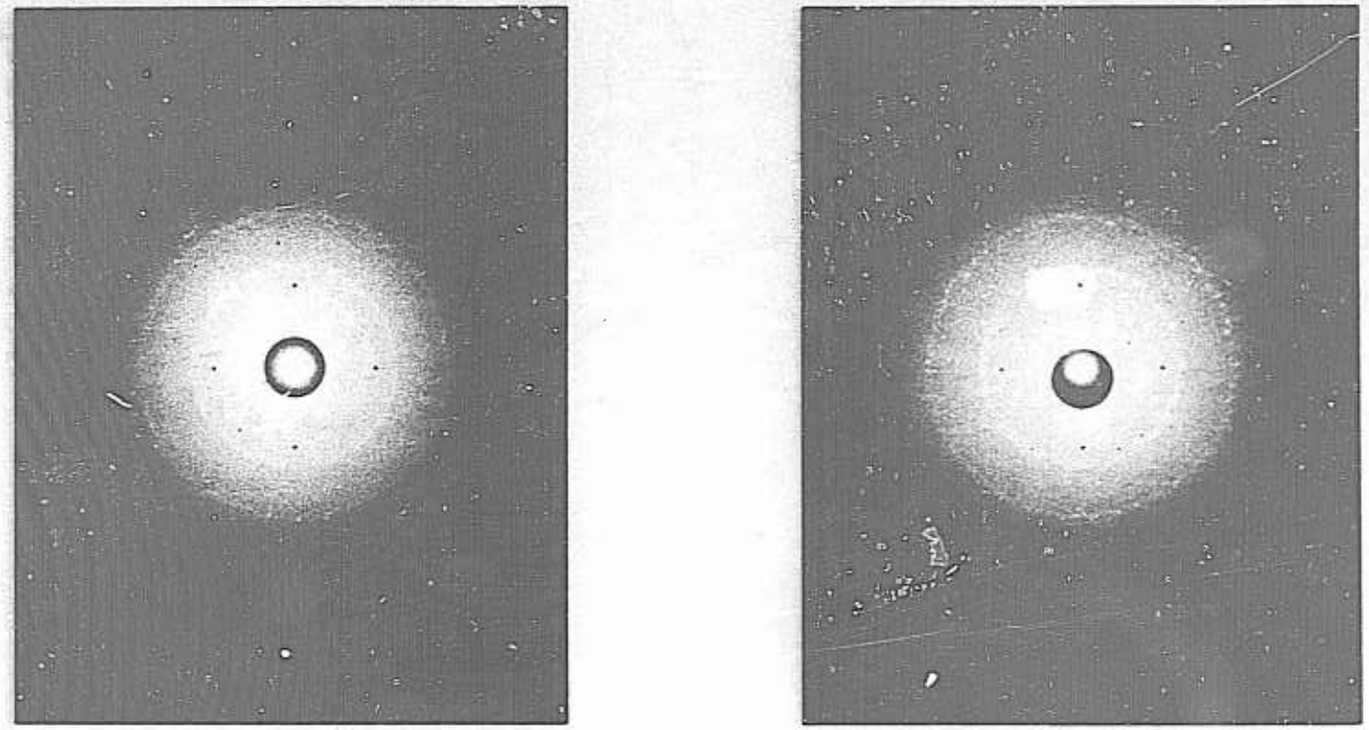

(a) R = 0 (b) R = 40

Figure 29

EPITAXIAL ZnSe LAUE PATTERNS

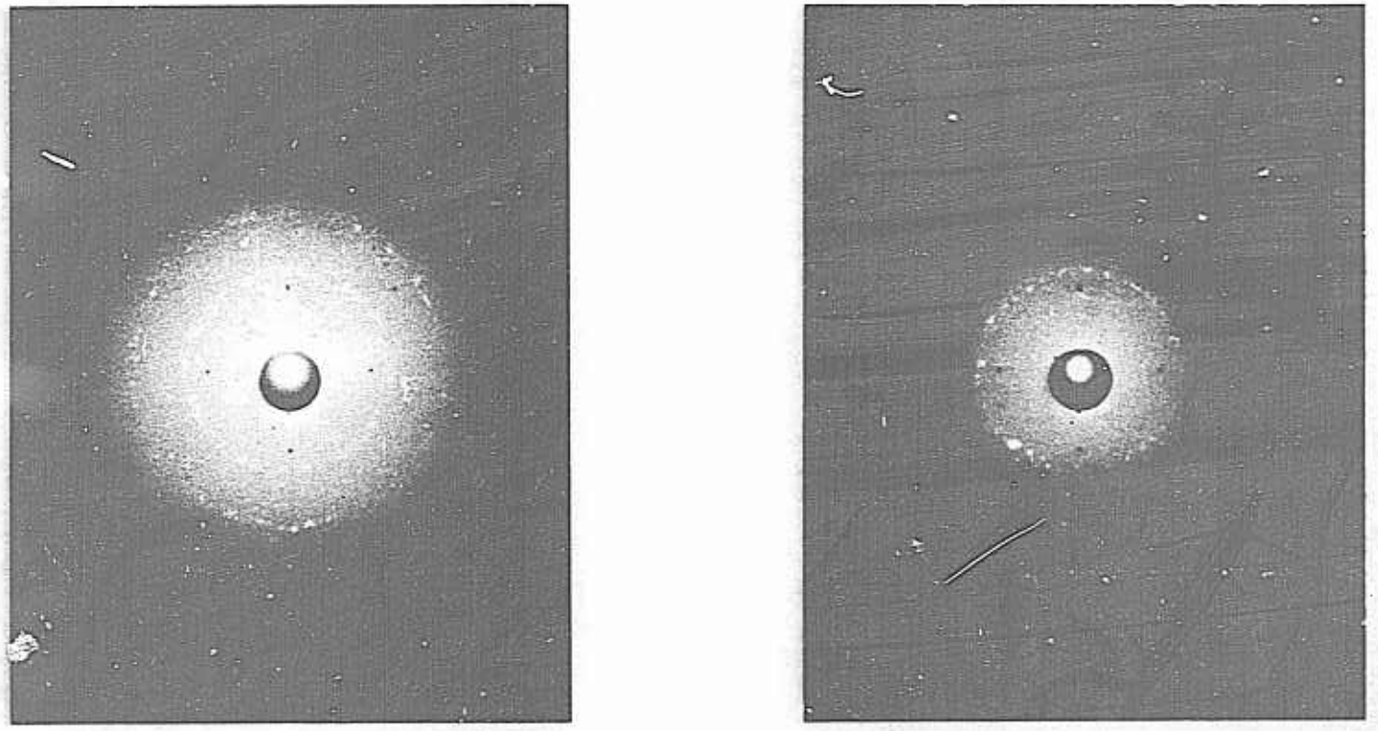

(c) R = 75 (d) R = 75

Figure 30

EPITAXIAL ZnSe LAUE PATTERNS

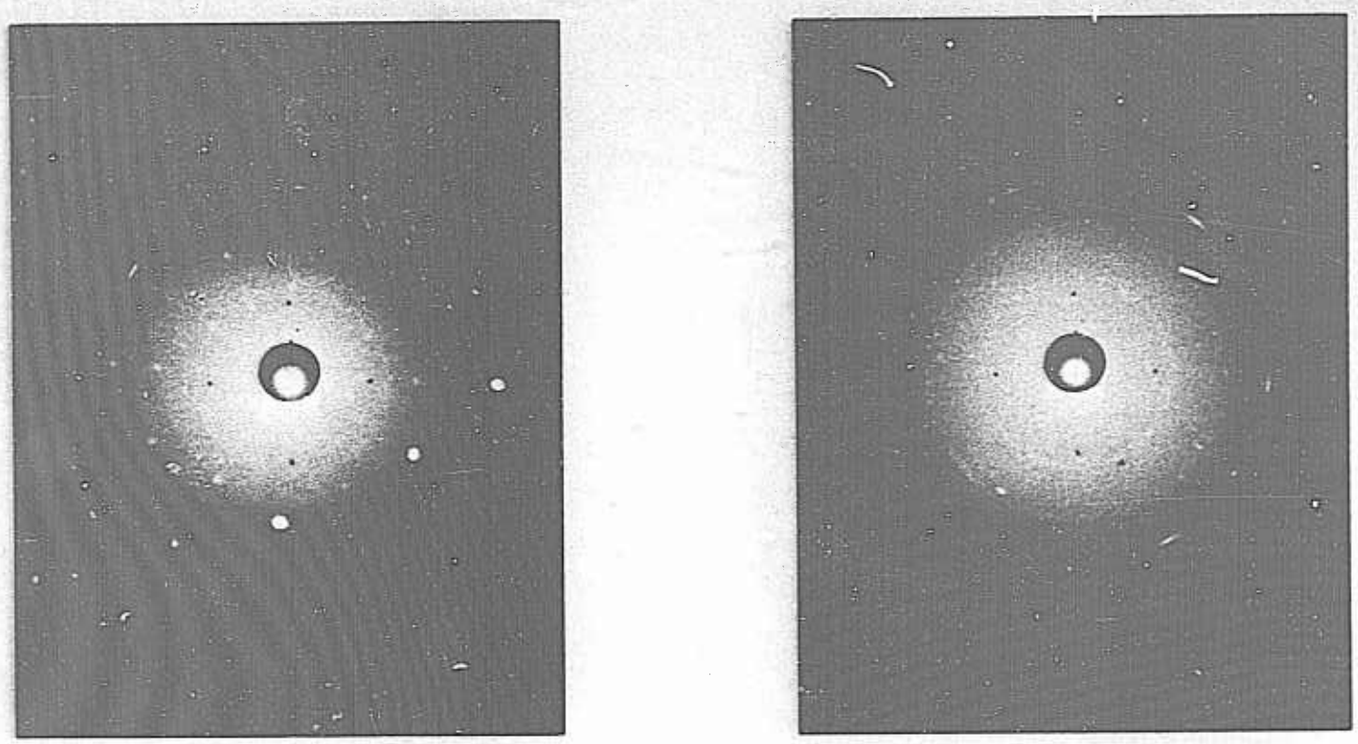

(e) THIN FILM (f) R = 50

Figure 31

EPITAXIAL ZnSe LAUE PATTERNS

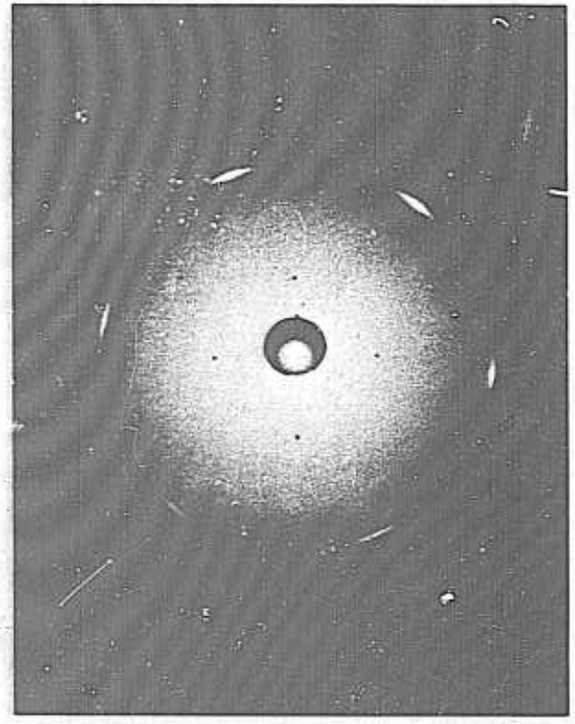

(g) R = 90

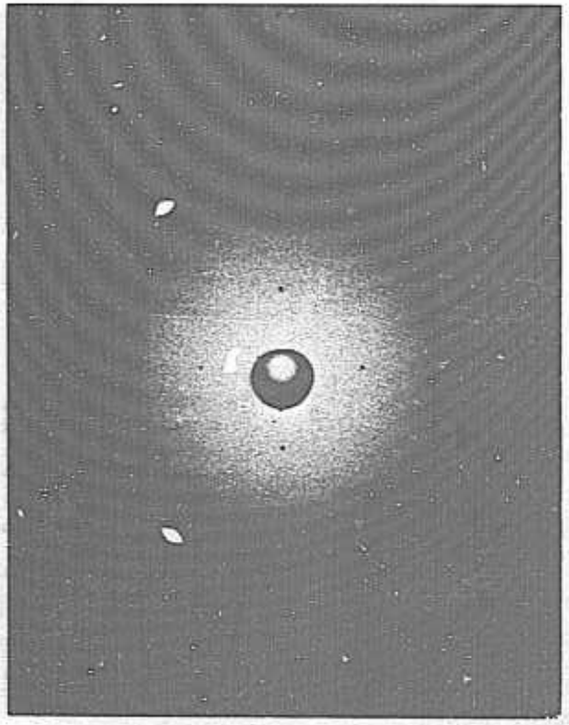

(h) R = 100

Figure 32

EPITAXIAL ZnSe LAUE PATTERNS

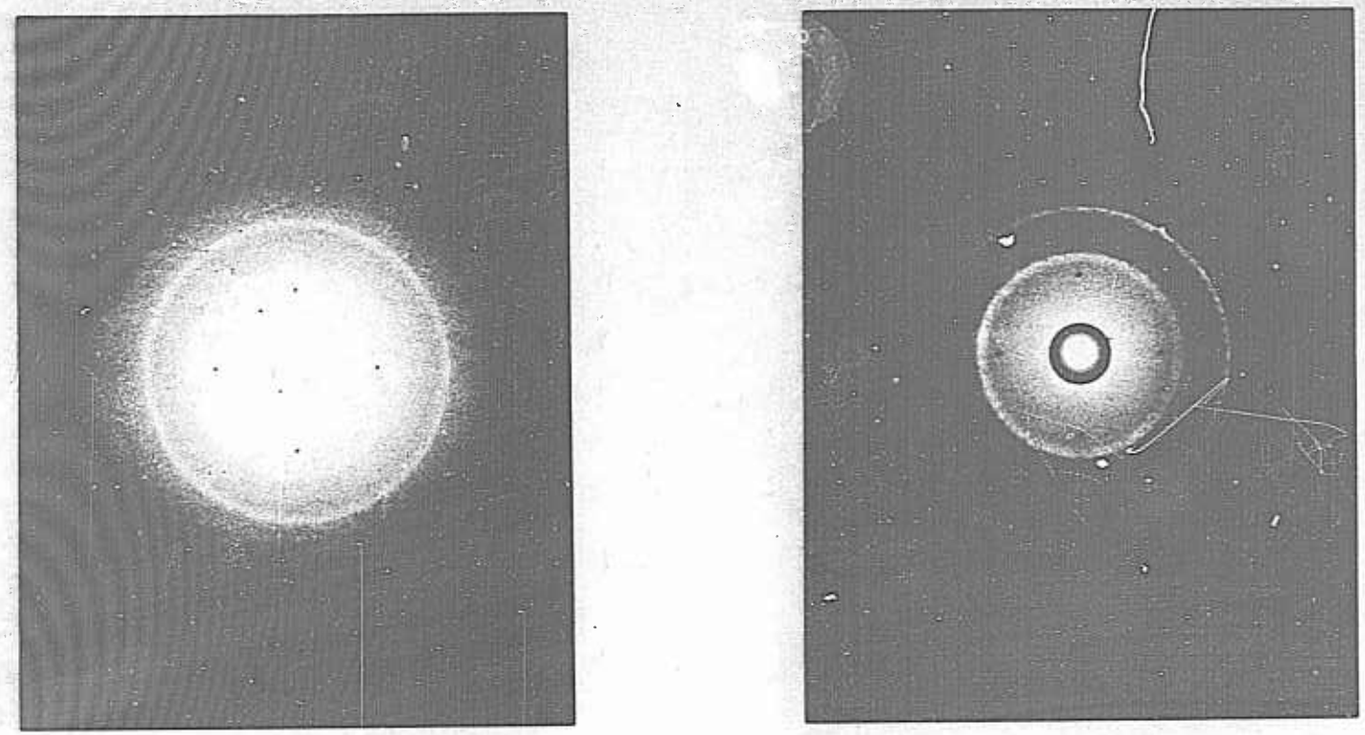

Figure 33

EPITAXIAL ZnTe LAUE PATTERNS

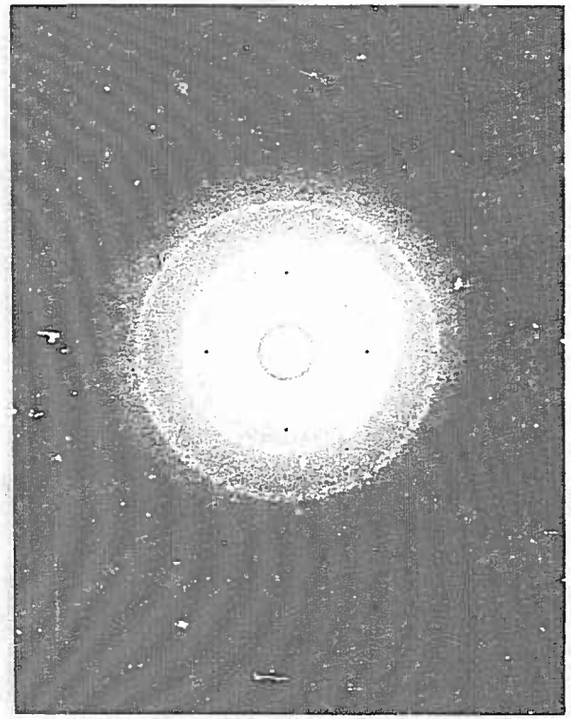

(c) R = 75

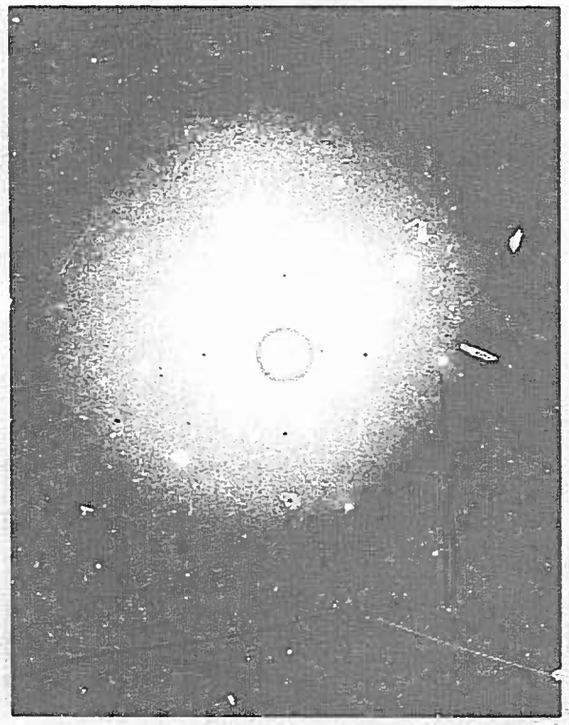

(d) T_c = 400°C R = 100

Figure 34

EPITAXIAL ZnTe LAUE PATTERNS

Figure 32 (g) shows only the main plane of the cubic phase with the threefold symmetry of < 111 > ZnSe well defined; although monocrystalline structure is not attained, a clear tendency to three dimensional organization is visible. (h) with the slightly elongated spots indicates a near perfect epitaxy at a substrate temperature of 400°C. This film contains only the cubic phase.

The following conclusions summarize the observations made. Increased concentration in the impinging vapor favors the formation of the hexagonal phase, as does condensation at low substrate temperature. A pure hexagonal phase could not be obtained within the angle of incidence achieved in this work. Grazing incidence to produce the hexagonal modification[18] was not verified in this work.

The hexagonal phase has been found to be more sensitive to composition of the impinging vapors. Excess Se assists in forming a pure cubic phase, which is the only structural phase found in the films at temperatures above 400°C.

On etched sapphire substrates cut in the < 0001 > plane, ZnSe films, well adherent, have been grown up to 0.040" thickness. Similar procedure has been applied to ZnTe, whose function is shown in Figure 28 (b); the influence of substrate temperature on crystallization is shown in Figures 33 and 34. The perfect structure of the epitaxial film on sapphire shown in Figure 34 (d) has been obtained at a condensation temperature, above the value at which epitaxy sets, presently at 425°C.

6. ELECTROLUMINESCENT DEVICES

a. Constraints in II-VI Devices

As stated earlier, amphoterism is not achievable in large band gap materials, at least to an extent where comparable conductivities for both p & n type of carrier are obtained. The availability of radiative centers will therefore be proportional to the lowest of the two concentrations.

All desirable II-VI compounds are predominantly n type, except for ZnTe, the only p type material in the series, which, however, has a lower conductivity and is a poor phosphor.

Dissimilarities, in band gaps, in lattice spacings, in electronegativities, in solubility of dopants, in thermal coefficients of expansion, have prevented the formation of abrupt homojunctions by alloying ZnTe with another II-VI compound - ZnTe heterojunctions formed with CdS[9] [19], or, with ZnSe[20][21], present broad heterojunctions. Similarly, a ternary compound $ZnSe_xTe_{1-x}$ [22][23], still has most of these shortcomings and radiates only in the yellow part of the spectrum. This alloying has not been successfully achieved in film form during the course of this work.

All broad heterojunctions have high ohmic resistance and, consequently, broad junctions are not efficient devices. They need the flow of very high currents to become efficient; such restriction of course makes their usability questionable.

The reduction of ohmic losses requires high conductivity and very thin p and n regions. The former requirement is hardly achievable when deep levels are introduced in the band gap by doping impurities.[24] Only at very high concentration can impurity bands merge with the main band and improve the efficiency at high currents; this, however, lowers the junction efficiency at low exciting voltage. Ultimately the maximum conductivity will be limited by solubility and segregation coefficients of doping impurities.

Until better interfacing between p and n, II-VI compounds can be secured with still unknown methods in exploiting defects chemistry, these heterojunctions will remain inefficient devices.

b. Heterojunctions Produced

Two different types of heterojunctions were investigated during this work, one based on a p i n structure, the other using a I-VI compound as the p type region.

(1) Pin Structure

The first type of junction investigated had a co-planar configuration with electrodes of indium and platinum side by side onto a film of gallium doped ZnSe. A similar approach has already been discussed[25]; it relies upon a potential barrier created by a high work function metal in contact with ZnSe viz. ZnSe-Pt. The other electrode material has a low work function which results in an ohmic contact with the semiconductor.

The height of the potential barrier, Φ, through which the charge carriers gain their kinetic energy is expressed by[26],

$$q V_D = \Phi = \phi_m - \phi_s \qquad (25)$$

with: V_D the diffusion potential; q the elementary charge; ϕ_m the metal work function; ϕ_s the semiconductor work function, $\phi_s = X + E_F$, where $X = \Phi - EG = \phi_s - E_F$, with X , Eg, and E_F respectively the semiconductor electron affinity, its band gap and Fermi level.

The surface state influences profoundly the work functions of both metal and semiconductor; as a result, the potential barrier is seldom calculable from the work function alone.

The characteristics of such junction are accessible through barrier capacitance measurements from derivation of Poisson's equation

$$\frac{d^2 \psi}{d x^2} = - \frac{qNd}{\epsilon \epsilon_o} \qquad (26)$$

with: $\psi = (V_D + V)$ at $x = d$; d the barrier thickness, V the applied voltage; Nd the donor density; ϵ the dielectric constant of ZnSe; ϵ_o free space permittivity, we have,

$$(V_D + V) = \frac{q\ Nd}{2\ \epsilon\epsilon_o}\ d^2 \tag{27}$$

since the charge Q for unit area is,

$$Q = q\ Nd\ d$$

$$= \left[2\ \epsilon\epsilon_o\ q\ Nd\ (V_D + V)\right]^{\frac{1}{2}} \tag{28}$$

the junction capacitance follows from,

$$c = \frac{dQ}{dV} \tag{29}$$

$$= \left[\frac{q\epsilon\epsilon_o Nd}{2(V_D + V)}\right]^{\frac{1}{2}}$$

the thickness of the barrier is obtained from eq (27) as,

$$d = \left[\frac{2\epsilon\epsilon_o}{q\ Nd}\ (V_D + V)\right]^{\frac{1}{2}} \tag{30}$$

eq (28) may be written in the form,

$$\frac{d(1/C^2)}{dV} = \frac{2}{q\ \epsilon\epsilon_o\ Nd} \tag{31}$$

from which the carrier concentration gives

$$N_d = \frac{2}{q\ \epsilon\epsilon_o}\ \frac{dV}{d(1/C^2)} \tag{32}$$

extrapolating $1/C^2$ to zero gives the value of the diffusion potential V_D.

The current voltage relationship in such electroluminescent diode is represented by,

$$I = Io\ (\exp - \frac{qV}{kT} - 1) \tag{33}$$

where the saturation current Io is obtained from the equation,

$$Io = \left(\frac{4\ \pi\ q\ m^* k^2}{h^3}\right) T^2 \exp -\left(\frac{\phi\ m - X}{kT}\right) \tag{34}$$

with m* the effective mass; k Boltzmann's constant; h Planck's constant; T the temperature.

The probability of generating electroluminescence by field ionization, when operating the diode in the reverse direction may be calculated from[27],

$$p = \frac{q\ E\ dn}{h} \exp \left[- \frac{\pi^2}{2\ q\ h\ E} \sqrt{2m^*}\ Eg^{3/2} \right] \tag{35}$$

with: E the field strength $E = \frac{2(VD + V)}{d}$ across the junction; dn the nearest neighbor distance $dn \frac{a_o\sqrt{3}}{4}$ with a_o the lattice constant of ZnSe a_o = 5.658A

Measurements were performed with a Booton bridge at 1 Mc sec^{-1} with a builtin D.C. power supply providing the voltage V. The capacitance of a junction area approximately 5 x 10^{-3} cm^2 has been plotted as a function of voltage, Figure 35 (a) introducing the constants ϵ = 8.7 for ZnSe; ϵ_o = 8.85 x 10^{-14} Fd. cm^{-2} in the function $1/C^2 = f(V)$ yields a carrier concentration Nd $\approx 10^{18}$ cm^{-3} with about one order of magnitude discrepancy from resistivity measurements. From extrapolation of Figure 35 a diffusion voltage of 1.98 volt is found, whereas extrapolating the function current - voltage, Figure 36, a value of 2.1 volts is obtained; the discrepancy between the two values is small and well within the errors due to the small junction area. With a barrier's thickness calculated from eq (30) $\approx$ 4 x 10^{-4}cm the probability from eq (35) approaches unity as the voltage approaches 20 volts.

The current voltage relationship for the diodes tested is shown in Figure 36 and emission spectrum plotted at room temperature in Figure 11.

The brightness has been measured by bringing in the vicinity of the diode surface a fiber optics coupled with the photomultiplier of a Gamma photometer. The brightness has been plotted as a function of the diode current in Figure 37. This plot indicates a light intensity proportional to the current within the range of current investigated.

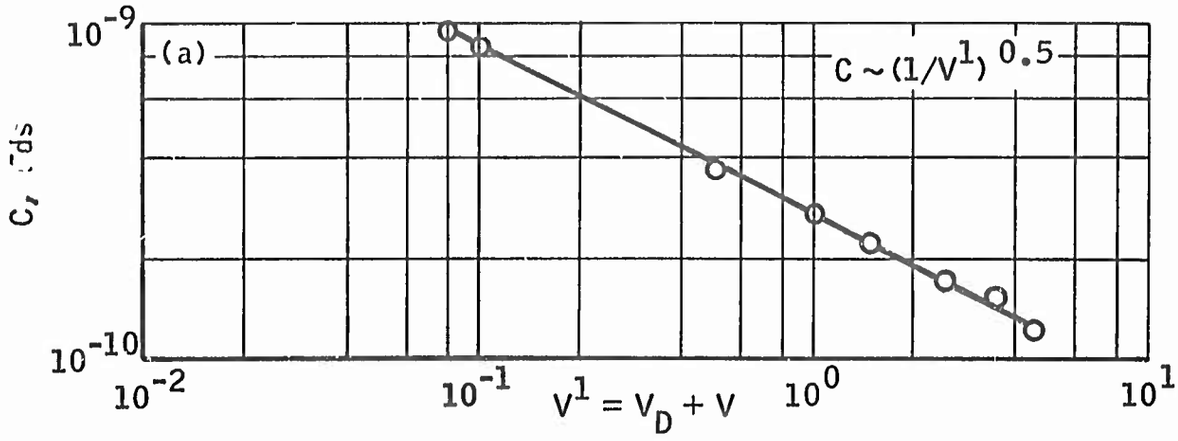

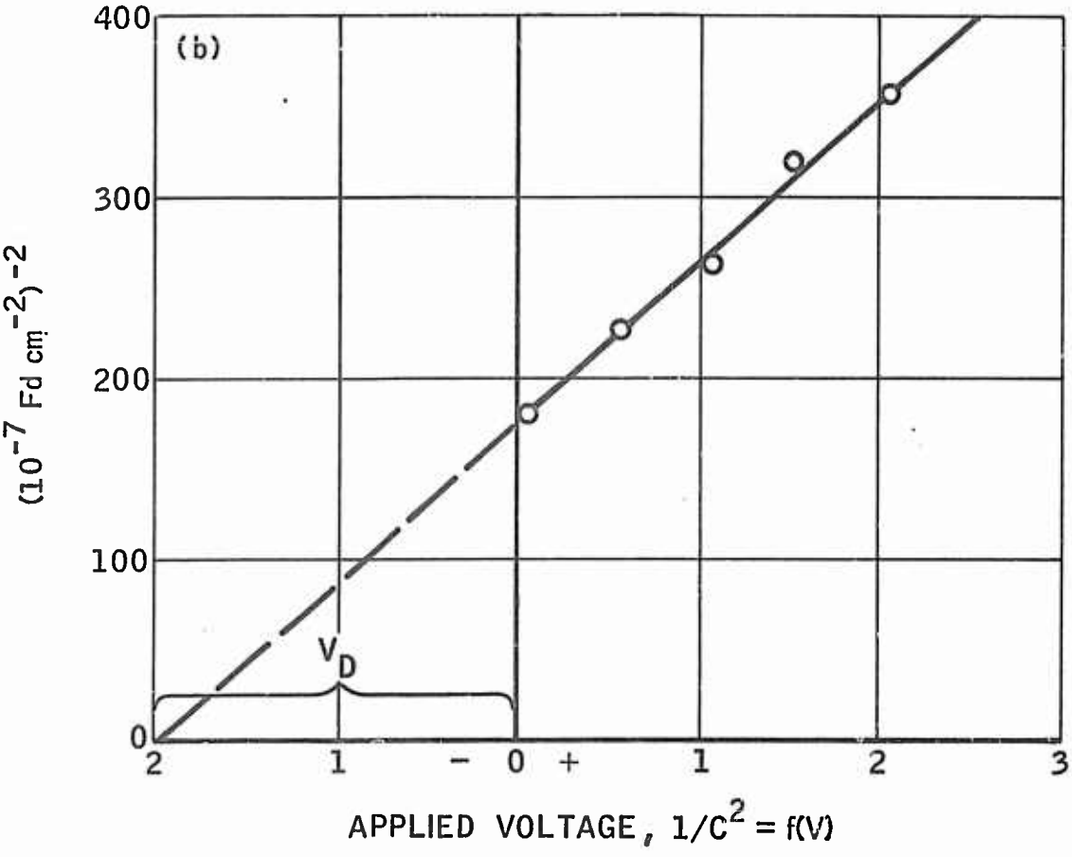

Figure 35

CAPACITANCE vs. VOLTAGE ACROSS JUNCTION

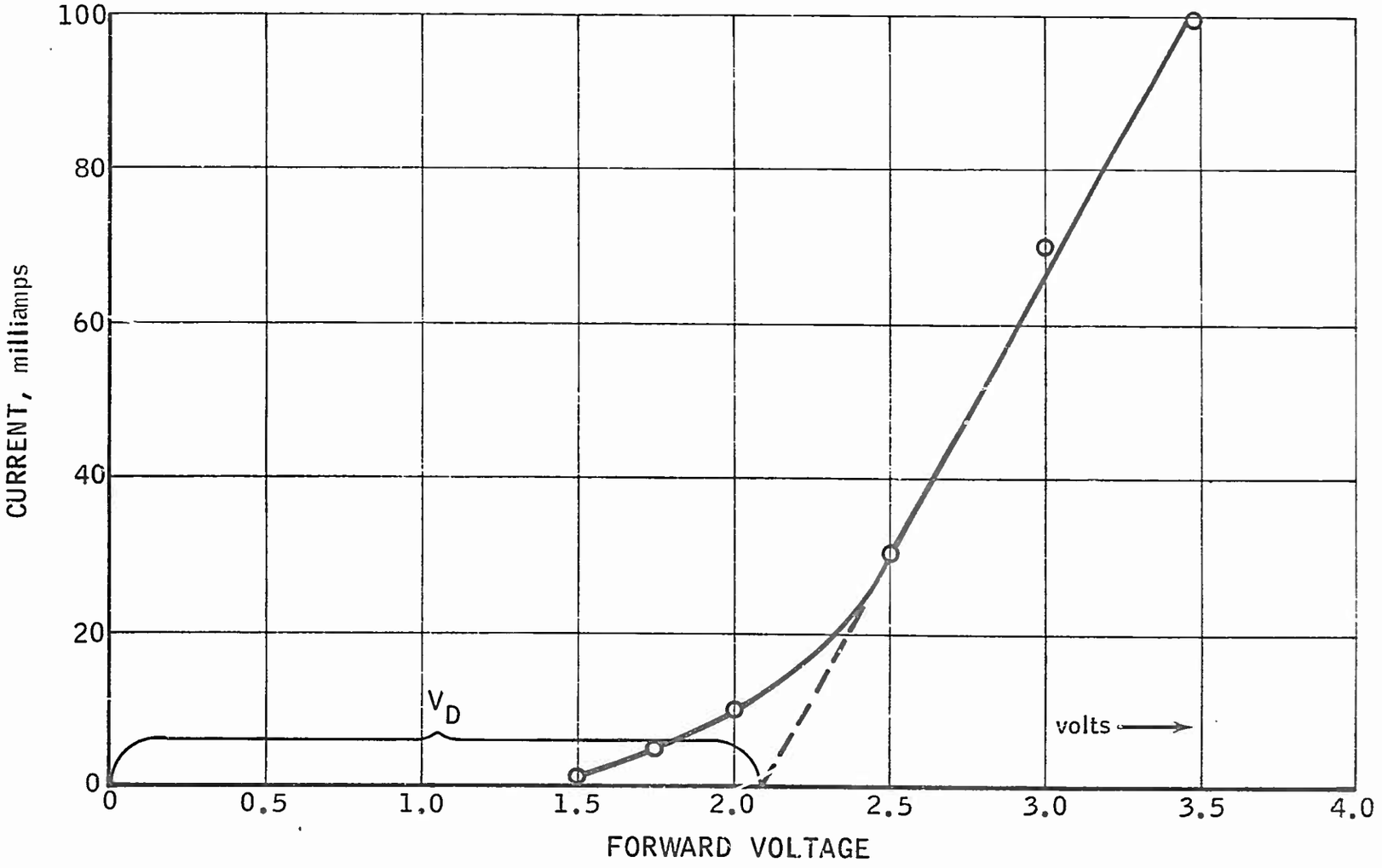

Figure 36

pin DIODE VOLTAGE-CURRENT RELATIONSHIP

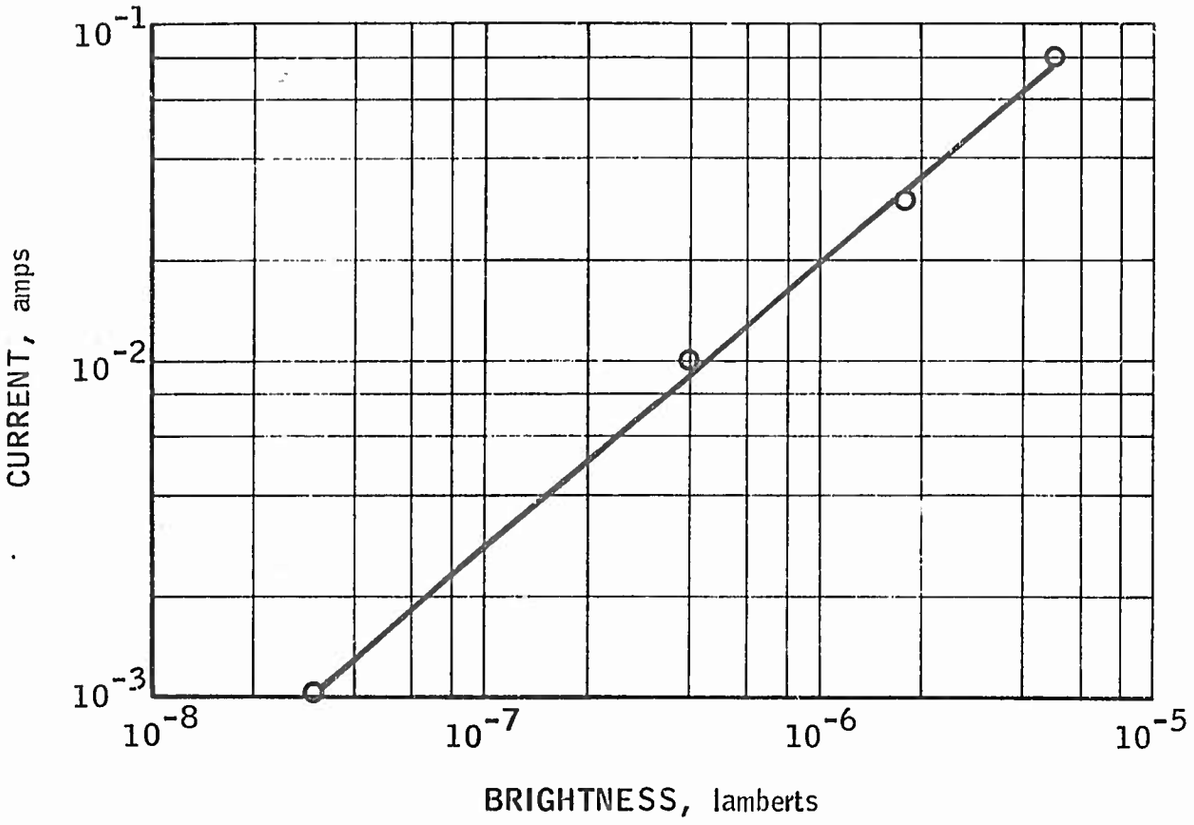

Figure 37

CURRENT-BRIGHTNESS RELATIONSHIP

The efficiency of the electroluminescent diode was evaluated, taking into account the spectral response and the steradiancy between junction's plane and fiber optics from eq (22) as a function of the current in the diode.

The measurements were repeated within the linear range shown in Figure 37 to give

$$\frac{\phi}{i} \times 100 = \text{efficiency in percent} \tag{36}$$

with i the current in amperes.

The efficiency of the diode tested was found to vary between 0.1 to 0.05 percent, i.e., 10^4 more electrons per photons.

(2) III-V - II-VI Structure

This form of heterojunction is expected to provide a set of conditions more favorable for an efficient injection mechanism than existing in other models.

Heterojunctions based on other than II-VI compounds, for example, Cu_2Se - ZnSe have already been experimented with[28] and alleged to have the same order of output and efficiency as the pin junction. The conductivity of 30 mhos of p type copper chalcogenide deposited upon ZnSe crystals can provide a higher hole injection rate than from ZnTe. Furthermore, near pseudo epitaxy can be effected between Cu_2Se and ZnSe since both belong to the same crystalline space group with nearly identical lattice spacings. In fact, the mismatch between nearest neighbor distances amounts only to 2 percent. However, a large band gap discrepancy exists between the two compounds, although Cu_2Se is not precisely known and does not fit the results from[29]

$$Eg = C \frac{Na-Nc}{Zc+Za} \tag{37}$$

with N valence and Z atomic number of cation and anion with C = 43 for Eg in e.v.

The value of 0.5 - 0.7 e.v. assumed[28] on the other hand fits the difference in electronegativities.

The optical properties of Cu_2Se imply a very poor external efficiency for this structure, somewhat lower than those obtained with the worse of the p i n junctions tested.

In an attempt to provide a high hole injection into n type ZnSe investigation was directed towards a structure based on the combination AlAs - ZnSe.

Aluminum arsenide is a p type semiconductor with a hole density of 10^{20} cm^{-3}; it has a crystal structure and nearest neighbor distances identical to ZnSe[30]. Both ZnSe and AlAs have nearly identical coefficients of expansion and hardness; the indirect band gap of 2.25 e.v. of the later compound should provide a much better fit with ZnSe than Cu_2Se does.

The bulk of the effort devoted to this approach was directed towards the epitaxy of both compounds and the formation of films of compatible thickness.

Little data has been published on this highly reactive compound and some difficulties have been experienced during its vacuum evaporation.

SECTION IV

CONCLUSIONS

The work performed during the previous phases of this contract covered the development of thin films of photoconductor and ferroelectric materials. During the present period the effort was oriented toward the production of a non-aging electroluminescent diode capable of driving the photoconductor-ferroelectric ASP model.

From the experimental results gathered it is concluded that low voltage electroluminescence is a possible means of control in switching photoconductor-ferroelectric ASP elements as indicated by analysis.

It is further concluded that electroluminescent materials operable at low voltage can be implemented by thin film deposition techniques. Experiments have verified that the production of electroluminescent materials was compatible with the preparation of photoconductor-ferroelectric materials in film form.

The present state of the electroluminescent thin film development does not, however, offer compatibility, on an energy basis, between electroluminescent-photoconductor-ferroelectric materials.

Experimental results show that storing or retrieving one bit can be made with less than 10^{-4} ergs, whereas with the present electroluminescent function this level of energy is raised to 150 ergs.

It is, therefore, concluded that in order to exploit fully the merits of photoconductor-ferroelectric ASP, improved performances must be achieved in the electroluminescent junction. Such improvement in the electroluminescent junction characteristics can be expected with additional development effort on the diode structure.

SECTION V

REFERENCES

1. A. N. Nesmeyanov, "Vapor Pressure of the Elements", Academic Press (1963).
2. D. R. Stull and G. C. Sinke, Adv. in Chem. Series #18, Amer. Chem. Doc. (1956).
3. M. Kahayashi, Intern. Z. Metallog, 2-65 (1912).
4. J. Carides and A. G. Fisher, Solid State Comm., 2-217 (1964).
5. A. G. Fisher, J. Electrochem. Soc., 106-838 (1959).
6. S. Narita, H. Harada, K. Nagasaka, J. Phys. Soc. Japan, 22-1176 (1967).
7. L. C. Greene, D. C. Reynolds, S. J. Czysack, W. M. Baker, J. Chem. Phys., 29-1375 (1958).
8. W. W. Piper, S. J. Polish, J. Appl. Phys., 32-1278 (1961).
9. M. Aven, W. Garwacki, J. Electrochem. Soc., 110-401 (1963).
10. D. B. Holt, Brit. J. Appl. Phys., 17-1395 (1966).
11. H. M. Manasevit, J. Electrochem. Soc., 115-434 (1968).
12. Swanson & Fuyat, NBS Circular 539, Vol. III (1953).
13. NBS Monograph, 25-3 (1964); Spinulescu-Carnaru Phys. Status Solidus, 18-269 (1966).
14. Geological Survey Circular, 29 August (1948).
15. H. Kidesy, Am. Min., 39-750 (1954).
16. H. P. Klug, L. E. Alexander, X-ray Diffraction Procedure, J. Wiley (1954).
17. S. Ino, D. Watanabe, S. Ogawa, J. Phys. Soc. Japan, 19-881 (1964).
18. K. V. Shalimova, A. F. Andrushko, J. Dima. Sov. Phys. Cryst., 10-414 (1966).
19. M. Aven, D. N. Cook, J. Appl. Phys., 32-960 (1961).
20. M. Aven, Appl. Phys. Letters, 7-146 (1965).
21. M. Aven, W. Garwacki, J. Appl. Phys., 38-2302 (1967).
22. S. Larack, R. Schrader, C. Stocker, Phys. Rev., 108-587 (1957).
23. M. Aven, Appl. Phys. Letters, 7-146 (1965).
24. M. Aven, B. Segall, Phys. Rev., 130-87 (1963).
25. A. G. Fisher, Phys. Letters, 12-313 (1964).
26. H. K. Henish, Rectifying Semiconductor Contacts, Clarendon Press (1957).
27. A. N. Georgobiani Opt. Spectry (USSR) Eng. Transl., 11-231 (1961).
28. M. Aven, D. A. Cusano, J. Appl. Phys., 35-606 (1964).
29. R. H. Bube, Photoconductivity of Solids, J. Wiley (1960).
30. G. Giesecke, Semiconductors, Vol. 2, Academic Press (1966).

UNCLASSIFIED
Security Classification

DOCUMENT CONTROL DATA - R & D

(Security classification of title, body of abstract and indexing annotation must be entered when the overall report is classified)

1. ORIGINATING ACTIVITY *(Corporate author)* The Marquardt Corporation 16555 Saticoy St., Van Nuys, CA 91409	2a. REPORT SECURITY CLASSIFICATION Unclassified 2b. GROUP

3. REPORT TITLE

Electro Optics for Associative Storage Processor

4. DESCRIPTIVE NOTES *(Type of report and inclusive dates)*

Final (12 March 1968 through 12 March 1969)

5. AUTHOR(S) *(First name, middle initial, last name)*

Jacques M. Hanlet

6. REPORT DATE	7a. TOTAL NO. OF PAGES	7b. NO. OF REFS
July 1969	58	30

8a. CONTRACT OR GRANT NO.	9a. ORIGINATOR'S REPORT NUMBER(S)
F30602-68-C-0199 b. PROJECT NO. 5581 c. 558109 d.	TMC Report No. 25,286 9b. OTHER REPORT NO(S) *(Any other numbers that may be assigned this report)* RADC-TR-69-119

10. DISTRIBUTION STATEMENT

This document is subject to special export controls and each transmittal to foreign governments or foreign nationals may be made only with prior approval of RADC (EMIIO), GAFB, N.Y. 13440.

11. SUPPLEMENTARY NOTES	12. SPONSORING MILITARY ACTIVITY
	Rome Air Development Center (EMIIO) Griffiss AFB, NY 13440

13. ABSTRACT

A research and development program to develop materials and investigate their use in an electro optical associative processor. An analysis is performed to determine the compatibility between ferroelectric-photoconductor and light source from an energy viewpoint.

The material effort directed toward the development of thin film carrier injection electroluminescent materials is presented. The effort culminated with definition of a fabrication process for a P I N electroluminescent cell that can switch a ferroelectric element carrying a charge of approximately 10^{-9} micro-coulombs in 30 microseconds.

DD FORM 1 NOV 65 1473

UNCLASSIFIED
Security Classification

14. KEY WORDS	LINK A		LINK B		LINK C	
	ROLE	WT	ROLE	WT	ROLE	WT
Associative Processor						
Associative Memory						
Thin Film Materials						
Photoconductor						
Ferroelectric						
Electroluminescent						

AFLC—Griffiss AFB NY 11 Aug 69-77